THESIS FOR THE DEGREE OF LICENTIATE OF ENGINEERING

# Dynamics of Enzyme Immobilization in Mesoporous Silica Particles

Pegah S. Nabavi Zadeh


Department of Chemistry and Chemical Engineering
CHALMERS UNIVERSITY OF TECHNOLOGY
Gothenburg, Sweden 2015

Dynamics of Enzyme Immobilization in Mesoporous Silica Particles

PEGAH S. NABAVI ZADEH



Chalmers Tekniska Högskola

Licuppsatser vid Institutionen för Kemi and Kemiteknik. 2015:13

ISSN: 1652-943X

Department of Chemistry and Chemical Engineering

Chalmers University of Technology

SE-412 96 Gothenburg

Sweden

Telephone + 46 (0) 31-772 1000

Cover: A graphical illustration of real-time monitoring of enzyme immobilization into a porous particle with hexagonally structured pores. The interaction of labelled-enzymes with mesoporous particles is observed as an increase in emission intensity (gray line) compared to a sample with no particle (black line).

Printed by Chalmers Reproservice

Gothenburg, Sweden, December, 2015

*"A journey of a thousand miles begins with a single step"*

*Lao Tzu*

Dynamics of Enzyme Immobilization in Mesoporous Silica Particles

*Pegah S. Nabavi Zadeh*
Department of Chemistry and Chemical Engineering
Chalmers University of Technology

ABSTRACT

The focus of this thesis is placed on the dynamic behavior of proteins in confining environments which is studied as a scientific challenge for a deeper understanding of the immobilization mechanism and a better designing of enzyme immobilization in porous materials. Enzymes are immobilized in porous materials to improve the enzyme activity and simplify their purification from the product solution in biocatalytic applications. Mesoporous silica particle is used as solid support material for immobilization of enzymes. By using various spectroscopic techniques it is possible to probe the environment that enzymes experience inside the pores and/or outer surface of solid porous materials in terms of pH, polarity and characterize the behavior of enzymes after attaching or during the immobilization process.

The two papers presented in this thesis are an effort to get closer to the mechanistic steps of immobilization process. In the first paper, a fluorescence spectroscopy assay based on dye-labelled proteins was proposed to monitor the whole immobilization process into mesoporous silica in real time. The main aim was to quantify the kinetics of the enzyme immobilization into mesoporous particles. And secondly it was investigated how the rate of the immobilization depends on protein size for a given pore size, the larger the protein the slower the rate.

The second paper described how the rotational motion of immobilized proteins is retarded compared to free proteins in solution by using steady state fluorescence anisotropy which was based on the intrinsic fluorescence of aromatic amino acids in proteins. The effect of the particle diameter and pore size on the mobility of immobilized enzymes were investigated and by calculating pore filling for each protein three possible mechanisms for decrease in rotational mobility of immobilized proteins have been discussed.

**Keywords:**

Enzyme immobilization, mesoporous silica, fluorescence spectroscopy, fluorescence anisotropy, rotational mobility, kinetics, pore filling, rate of immobilization, real-time monitoring.

LIST OF PAPERS:

This thesis is based on the work presented in the following papers:

**I. A fluorescence spectroscopy assay for real-time monitoring of enzyme immobilization into mesoporous silica particles**
Pegah S. Nabavi Zadeh, Kassam Abdel Mallak, Nils Carlsson, Björn Åkerman
*Analytical Biochemistry 476 (2015) 51–58*

**II. Rotational mobility and pore filling of enzymes confined in mesoporous silica particles studied by fluorescence anisotropy**
Pegah S. Nabavi Zadeh, Björn Åkerman
*Manuscript*

CONTRIUTION REPORT

Paper I. Performed the second part of the experiments, analyzed the data and wrote the manuscript.

Paper II. Designed and performed all the experiments, analyzed the data and wrote the manuscript.

LIST OF ABBREVIATIONS

| | |
|---|---|
| BSA | Bovine serum albumin |
| DNA | Deoxyribonucleic acid |
| GOX | Glucose oxidase |
| HMM | Hiroshima mesoporous materials |
| MML | Mucor miehei lipase |
| MPS | Mesoporous silica |
| NIR | Near infrared |
| SBA-15 | Santa Barbara amorphous |
| SEM | Scanning electron microscopy |
| TEM | Transmission electron microscopy |
| Trp | Tryptophan |
| Tyr | Tyrosine |
| UV-visible | Ultraviolet–visible |

# CONTENTS

# 1. INTRODUCTION

Enzymes are always referred to as useful biological catalysts with a high chemo- and regioselectivity while applied under mild conditions, such as temperature, pH and pressure [1, 2]. Therefore, enzymes can be a suitable alternative instead of using conventional catalysts. However, enzymes in general have low stability and also it is difficult to recover them from the reaction media and making the reuse very limited [3]. To improve the use of enzymes in biocatalysts applications, immobilization of enzymes in mesoporous silica particles (MPS) has been introduced as a novel method two decades ago [4]. These mesoporous materials as immobilization support have unique advantages in three different aspects, structure, pore and surface. The porous structure allows for high loading of enzymes and also provides a protective environment where the enzymes often can tolerate higher temperature, extreme pH and more salt concentration [1, 4]. Also the size of particles can be adjusted for different applications which micrometer-sized mesoporous particles (up to 5 μm) are mostly used in biocatalyst applications [5]. The pore diameter can be selected to match with the size of the given enzyme, and the pore shape can be ordered in different shape, such as hexagonal or cubic [6]. The surface of the mesoporous materials can be modified, such as higher hydrophobicity to improve the enzyme activity and optimizing interaction between enzyme and support materials. Therefore, immobilization of enzymes in mesoporous materials improves the enzyme stability and enzymatic function, simplifies the biocatalyst recycling and enhances the product recovery [7, 8]

Enzyme immobilization has been studied at least in three main aspects, applied surface chemistry, industrial biotechnology and physical chemistry. However, in each aspect some main questions are raised, but the combined knowledge that is gained can help us design a better immobilization systems and have improvement in the applications. In applied surface chemistry, more focus is on the techniques used for the characterization of the MPS particles i.e. how to modify the surface in a way to enhance the system [9]. The biotechnology part is more focused on improving the role of enzymes after immobilization, optimizing the enzymatic activity and kinetics for biocatalyst application, investigating the modeling of the enzyme structure [10, 11].

The focus of this thesis is placed on the physical chemistry perspective of enzyme immobilization and most studies in this area have been trying to figure out the answers of

two questions, *"where are the proteins after immobilization?"* and *"what is the mechanism of the immobilization?"*.

To answer these questions, physical chemistry methods such spectroscopic techniques provide us this opportunity to know more about the environment that enzymes experience inside the pores or outer surface of the particles. Since polarity and pH of the environment can affect the enzyme functionality, they have been investigated by using different probes as protein-bound dyes which are sensitive to pH or polarity [12, 13].

The amount of immobilized enzymes can be crucial to their activity and dynamic behaviors [11, 14, 15] which can be determined by indirect methods (discussed further below) [16, 17], but if the adsorption of enzymes into support materials can be monitored over time, the rate of immobilization can be investigated. Since the estimation of adsorbed amount is often studied by indirect methods which have low time resolution, the necessity of developing the direct- monitoring method can be recognized. In the first paper of this thesis, a fluorescence assay is evaluated for real time monitoring of enzyme immobilization in mesoporous silica particles, and also making the kinetics of the immobilization quantified, this method can be a forward step to get close to the mechanism enigma.

In the second paper the dynamic behavior of immobilized enzymes is studied by measuring the depolarization of the enzymes after immobilization using fluorescence anisotropy, since the main source of the depolarization is internal protein motion and rotational diffusion, therefore, the mobility of immobilized enzymes can be quantified. The main aim is to determine the rotational mobility of immobilized enzymes since sometimes the catalytic activity can be completed by small fluctuational motions in enzymes [18].

Investigating the rotational mobility of immobilized proteins might seem like a contradiction in terms, but immobilization, here, means that the leakage into the external solution is prevented which sometimes referred to as encapsulation or confining enzymes in a solid materials, the translational motion of proteins is restricted highly but it does not mean that proteins cannot rotate inside the pores, depending on the mechanism and strength of the forces responsible for the immobilization.

# 2. MATERIALS

## 2.1. Enzymes

A catalyst is a substance that can increase the rate of a chemical reaction without itself being consumed or changing. Enzymes are biological catalysts that are highly selective in various chemical reactions. They can accelerate and regulate the metabolic reactions in the living cells. Without biocatalysts the chemical reactions in life processes, such as digestion of food and synthesis of DNA could last forever. Moreover, they can apply under very mild condition in terms of pH and temperature. The enzymatic reaction occurs in the active site where is a region on enzyme with specific amino acid residues which can bind to the substrate molecule. The reaction is catalyzed by chemical transformation of the substrate into a desired product [19].

Since the substrate selectivity of enzymes depends on interactions between enzyme and substrate, enzymes take advantage of many intermolecular forces including hydrogen bonding, van der waals interactions, polar interactions and hydrophobic interactions to bring substrates together in most optimal orientation so that reaction will occur. Enzymes as a catalyst just increase the rate of the reaction by decreasing the activation energy. Activation energy is the difference between the energy levels of the substrate ground state and the transition state. However, the equilibrium energy is referred to the difference in free energy between the ground states of substrate and product, which the catalyst cannot affect. There is an optimum pH for enzymes where they can achieve the highest catalytic activity due to different ionization state that amino acid residues can gain in different pH [20]. Naturally-occurring microorganisms (fungi and bacteria) are the most productive producers of enzymes since they are easy to handle, can be grown in huge tanks without light, and have a very high growth rate [20]. After purification process, enzymes are ready to be used in various industries e.g. biofuel cells, detergent formulations, biosensors, food and pharmaceuticals [21].

In this thesis lipase (MML), bovine serum albumin (BSA) and glucose oxidase (GOX) are used as “enzymes” in immobilization processes. Lipase and glucose oxidase both are recognized as the most important groups of enzymes in biotechnology. Lipase can be found in different bacterial strain and it plays the main role in metabolism and fat digestion. Glucose oxidase is found in some fungi and insects where it shows its antibacterial activity

in presence of oxygen and glucose. It catalyzes the oxidation of glucose to hydrogen peroxide and D-gluconolactine [22, 23].

Bovine serum albumin cannot be listed as an enzyme due to the lack of the active site in its structure. However, it is a well-known protein, which is usually used as a protein concentration standard in the lab experiments [24]. There are some reasons to choose BSA besides of others enzymes in this thesis, the main one is the size of the BSA (hydrodynamic radius ($R_H$): 3.5 nm) which is very suitable for comparing the data with other enzymes (MML, $R_H$: 2.25nm and GOX, $R_H$: 4.5 nm) in the immobilization process, and also it is suited with pore diameter of the used MPS particles ($R_{pore}$: 3nm and 4.6+/-0.2 nm). Figure 1 shows the schematic structure of the protein and Table 1 presents the proteins properties in detail.

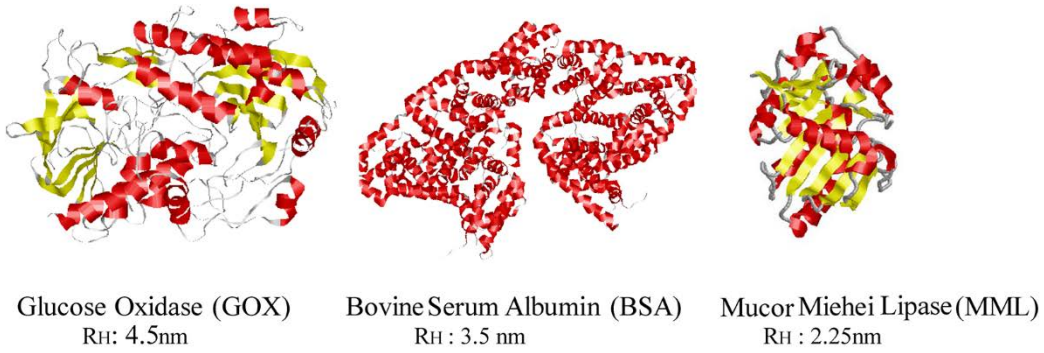


Figure1. Schematic representation of the proteins structure, Lipase (MML), Bovine Serum Albumin (BSA), Glucose Oxidase (GOX)

**Table1. Properties of the proteins**

| Protein [a] | $M_w$ [b] (kDa) | $R_H$ [c] (nm) | pI [d] | $\varepsilon_{280}$ [e] ($M^{-1}cm^{-1}$) |
|---|---|---|---|---|
| MML | 32 | 2.25 | 3.8 | 42800 |
| BSA | 66 | 3.5 | 4.7 | 43824 |
| GOX | 160 | 4.5 | 4.2 | 308000 |

a. MML- Mucor Miehei Lipase, BSA-Bovine Serum Albumin, GOX-Glucose Oxidase
b. Molecular weight [3, 22, 25]
c. Hydrodynamic radius [3, 12, 22]
d. Isoelectric point [3, 12, 22]
e. Extinction coefficient [12, 22, 23]

## 2.2. Mesoporous materials

Mesoporous materials are defined as inorganic materials with a pore diameter between 2 and 50 nm. Porous materials with pore diameter less than 2nm are defined as microporous and when the pores are larger than 50 nm in diameter the materials called macroporous. They have a large variety of properties that depends on their composition, pore shape and particle morphology [26]. Mesoporous solid particles mostly are oxides, such as silica ($SiO_2$) [27], alumina ($Al_2O_3$) [28] or titania ($TiO_2$) [29], and can be synthesized with regular symmetry. This thesis will focus on mesoporous silica particle (MPS), with the pores arranged in hexagonal symmetry, SBA-15 (*Santa Barbara Amorphous)* [22], and also HMM *(Hiroshima mesoporous material)* [30] which is a silica spherical particles with non-ordered pores with slit-shape.

Described briefly the MPS particles are synthesized from organic-inorganic self-assembly between the surfactant and the silica precursor in an aqueous solution. The silica precursor is hydrolyzed and polymerizes in the water domain of the template liquid crystal, it forms an inorganic network with mirroring the template structure. After polymerization, hydrothermal treatment is performed on the formed silica material for increased cross-linking, adjusting the pore diameter and particle growth. At the end, the organic template or surfactant is burnt away by calcination or extraction [31, 32].

Several analytical techniques are used to characterize the mesoporous materials. Scanning electron microscopy (SEM) is used to determine the morphology and the size of the MPS particles. Transmission electron microscopy (TEM) can be used as a complement to SEM for determining the local pore structure. Nitrogen adsorption/desorption isotherms can measure the surface area, pore volume and the pore size distribution in the MPS particles [30, 33].

Enzymes can be immobilized into mesoporous silica particles by covalent attachment or by physical adsorption and electrostatic interaction between the enzyme and the surface. For covalently attaching usually the surface is modified by functionalizing the silanol (SiOH) groups on the surface [34]. In physical adsorption multitude weak forces such as hydrogen bonds are involved between the enzyme and the surface. This interaction can be improved if there is electrostatic attraction between the enzyme and the silica surface. One way to

improve the immobilization conditions is changing the pH which may increase the electrostatic attraction [35, 36]. It is tuned by considering the isoelectric point of the enzyme, and the silica support (Silica pI~ 2). Some other parameters can affect the interaction between enzymes and the MPS particles such as enzyme properties in terms of primary, secondary, tertiary structure.

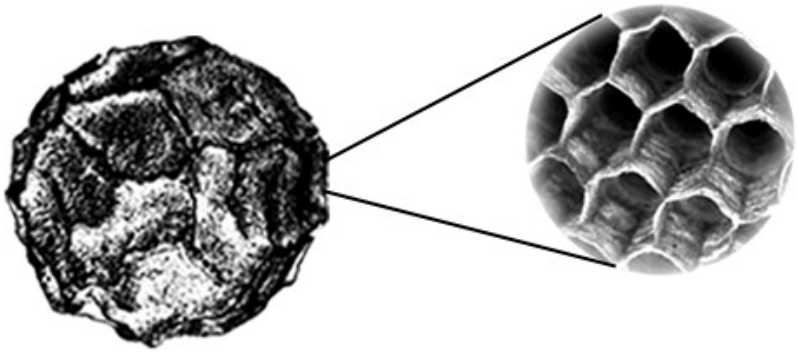

Figure 2. Schematic structure of MPS particles with uniform hexagonal pores.

# 3. METHODS

## 3.1. Light and matter

The electromagnetic spectrum lays out all in the different forms of radiation from very low energy like radio waves and microwaves to very high energy such as gamma rays and X-rays. But all electromagnetic radiation is not called light; light in a spectroscopic perspective is a strand of electromagnetic radiation between the lowest and highest energy that includes near-infrared (NIR), visible light and near or middle ultraviolet. To describe the properties of light, it must be considered a wave as well as a particle [37, 38]. In classical physics the light can be seen as a harmonic wave of an oscillating electric and magnetic field, the electric and magnetic fields oscillate in phase with a wavelength λ and frequency ν and describe waves which are perpendicular to each other and to the direction of propagation. However, the light can also be described as a flow of photons, small packets of energy E which can be quantified by Planck's equation

$$E = h.\nu \qquad (1)$$

where h is Planck's constant ($h=6.626.10^{-34}$ Js) and ν is the frequency which is connected to the speed of the light, c, as

$$\nu = \frac{c}{\lambda} \qquad (2)$$

where c=3.108 ($ms^{-1}$) and λ is wavelength of the light (nm).

This flow of photons can interact with matter in different ways, such as absorption and scattering or with no interaction just passing through the sample. The wavelength, the angle and polarization of the incoming light are the factors that choose to what degree each process can occur.

Molecules usually exist in different energy levels i.e. rotational, vibrational and electronic. This means that there is a particular energy difference between each level, and a molecule in an initial state can get excited to a final state if it absorbs a photon with exactly the amount of energy equal to the energy difference ΔE between both states. This is defined as Bohr´s frequency condition [39] and is given as

$$\Delta E = E_{Final} - E_{Initial} = h.\nu \qquad (3)$$

Transition dipole moment occurs when the oscillating electric field of light with the correct wavelength can create an oscillating in the electron cloud of a molecule, the molecule can

be excited from initial state to final state with a higher energy. This transition occurs with the highest efficiency if the electric filed of the light is polarized parallel to the transition moment and this dipole induced by light in the molecule determines the magnitude of the probability of this transition happening.

## 3.2. Absorption

Absorption is the ability of a molecule to absorb light energy when it is exposed in the light emitted by a source in a suitable wavelength. This ability is measured by spectrophotometer which includes a light source and a monochromator and a detector, see Figure 3.

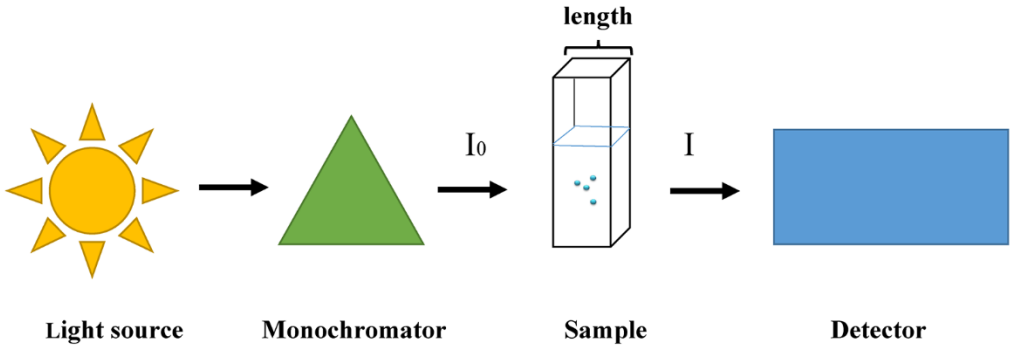


Figure 3. Basic setup of a spectrophotometer. The correct wavelength of the light is selected by a monochromator and goes through air ($I_0$) and then through a sample (I) with length (l) onto a detector.

The intensity of light decreases by passing through the sample and interacts with the molecules. The light intensity measured after the sample (I) is related to the incident light ($I_0$) at a certain wavelength (A). It is also related to the extinction coefficient (ε), the concentration (c) and the path length (l) of the sample (often in a quartz cuvette). This relation is described by Beer- Lambert law [40]:

$$A(\lambda) = log \frac{I_0(\lambda)}{I(\lambda)} = \varepsilon.c.l \qquad (4)$$

Absorption spectroscopy is often used to determine the concentration of a sample with a known extinction coefficient (ε), but for new molecules, the extinction coefficient can be determined experimentally by using a solution of known concentration. Otherwise for example for proteins it can be calculated from the amino acid composition data [41, 42].

## 3.3. Light scattering

In a complex sample (enzyme/particle) the total absorption consists of two component absorption and scattering which called turbidity. Scattering happens when the direction of a photon after interaction with the matter changes and it depends on the amount of particles in the sample which in scattering theory is often called number of particles per unit volume [43, 44]. To separation the scattering from absorption one way is the subtraction of the light scattering component from the total spectrum, then the absorbance part can be extracted. However, for extract the absorbance part, the scattering part must be identified. A convenient method to identify the scattering component is to use a logarithmic representation of the data. In a log-log graph the scattering signal will ideally appear as a straight line [45].

## 3.4. Fluorescence

When a molecule absorbs light, the energy is transferred from the photon to an electron. Electron with getting this energy can transfer to the higher energy orbital, and the molecule is located in the excited state. The excited state is unstable and the electron eventually return to the lower energy orbital and the molecule will be back in the ground state. However, the molecule has several options for losing this energy and returning to the ground state. According to Jablonski diagram (Figure 4) the energy can be given away to vibrational modes in the molecule (Internal conversion), it can be transferred to a triplet state (Intersystem crossing) or be emitted as a photon (fluorescence and phosphorescence). As it is seen in Figure 4, the molecule can be excited by using light at wavelength that corresponds to the energy difference between $S_0$ and $S_1$, The energy absorbed by the excited electron in $S_1$ can reveal to different vibrational modes; the energy in these vibrations is quickly transferred to the surrounding environment by non-radiative transitions (vibrational relaxation) so that the molecule is still in the lowest vibrational state in $S_1$, then the energy difference from $S_1$ to $S_0$ is emitted as fluorescence when the molecule goes back to the ground state $S_0$.

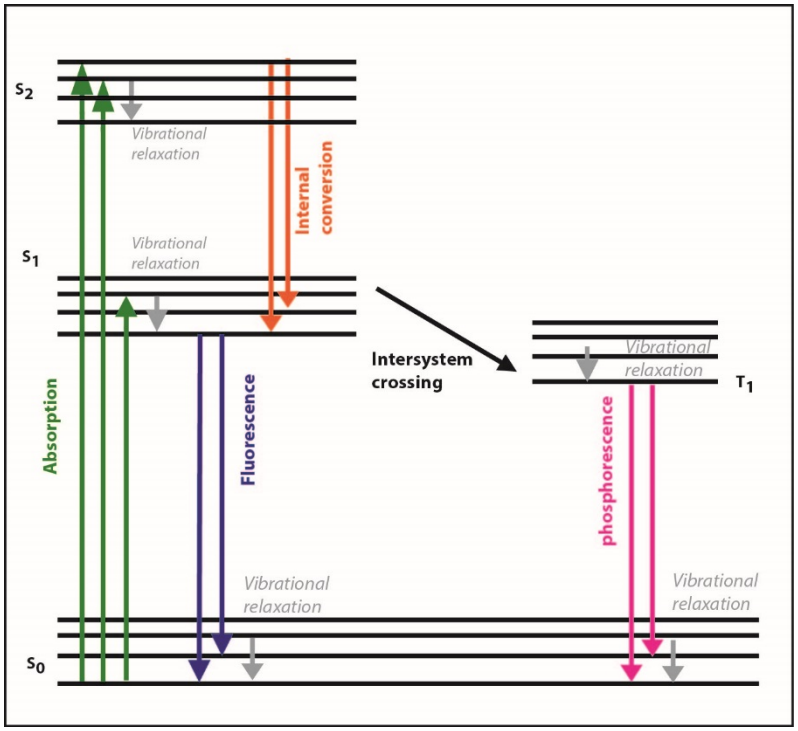


Figure 4. Jablonski diagram

Fluorescence quantum yield is a common measure for the fluorescence of a molecule, which is defined as the ratio between the number of photons emitted by a molecule as fluorescence and the amount of photons that is absorbed by the same molecule [45]. This relation can be described as:

$$\Phi = \frac{\Gamma}{\Gamma + k_{nr}} \qquad (5)$$

where Γ is the fluorescence rate constant and $k_{nr}$ is the rate of non-radiative decay to the ground state ($S_0$). The fluorescence rate constant in the relationship represent the photons emitted while the sum of rate constants make up for all transitions.

The fluorescence lifetime is another important parameter that is used to describe the photophysical behavior of the molecule, which is the average time the molecule spends in the excited state before emitting a photon. The lifetime is inversely proportional to the sum of rate constants involved in the transition from the excited state to the ground state [45]; lifetime equation can be described as following:

$$\tau = \frac{1}{\Gamma + k_{nr}} \qquad (6)$$

Figure 5 shows the basic setup of a spectrofluorometer, which is a common technique to record an emission and excitation spectra for a sample. The spectrofluorometer has a source

of UV-visible light that is directed through a monochromator by selecting the correct radiation energy to excite the sample. The emission monochromator selects the correct wavelength of radiation to be observed by the detector.

In the case that an emission spectrum is to be measured, a specific excitation wavelength will be chosen for the light source by the excitation monochromator which is then focused onto the sample. Photons are emitted by the sample and the emission monochromator is scanned through a chosen wavelength region, therefore, the detector can obtain a spectrum of the emission intensity per wavelength. An excitation spectrum is measured in a similar the same manner; however, this time the emission monochromator remains in a specific wavelength while scanning is through the excitation energies. Also kinetic studies are possible where only one wavelength (monochromatic light) is used and the intensity of the fluorescence can be recorded over time.

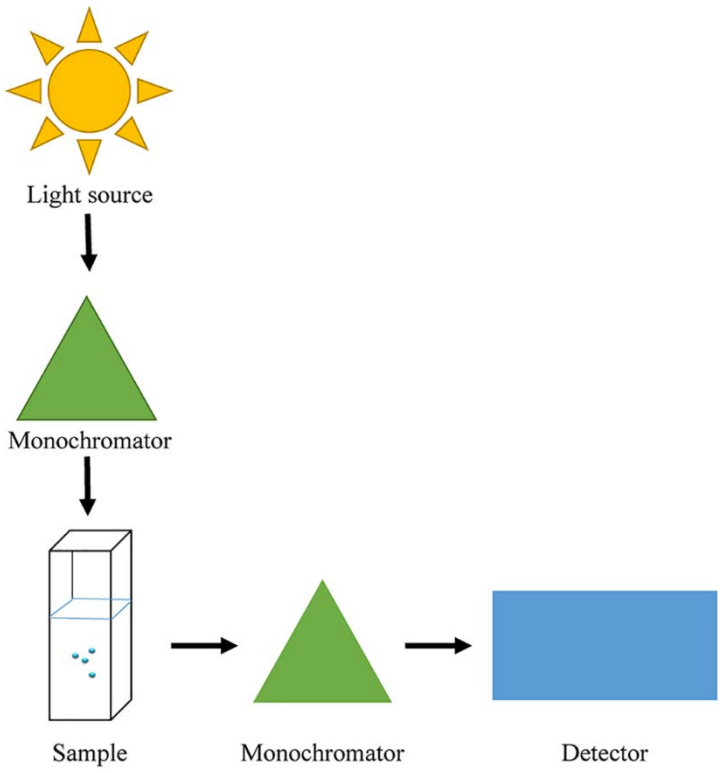


Figure 5. Basic setup of a spectrofluorometer. The correct wavelength of the light is selected by an excitation monochromator, led through the sample and then an emission monochromator and on to the detector.

### 3.5. Steady state fluorescence anisotropy

When a fluorescent molecule is excited with polarized light, the resulting fluorescence emission should be also polarized. But since the main cause of fluorescence depolarization is rotational diffusion of the fluorophore during its excited-state life, the emitted light is depolarized while the molecule rotates. Therefore, by measuring the fluorescence depolarization the rotational mobility of a fluorophore can be determined. Fluorescence anisotropy (r) is an experimental measure of fluorescence depolarization. Anisotropy measurements are made by exciting the fluorophore with polarized light and measuring the fluorescence intensity both parallel and perpendicular to the excitation polarization.

Figure 6 shows a fluorescence anisotropy spectroscopy setup with polarizers. Simply, the light passes a polarizer that only light in one orientation can be transmitted, such as vertically oriented light. The light excites a fluorescent molecule in the sample and by rotation of the molecule, the orientation of the emitted light changes. By using another polarizer, the light with the same orientation as the polarizer can pass completely through the filter and if it is perpendicular to the polarizer, it is blocked.

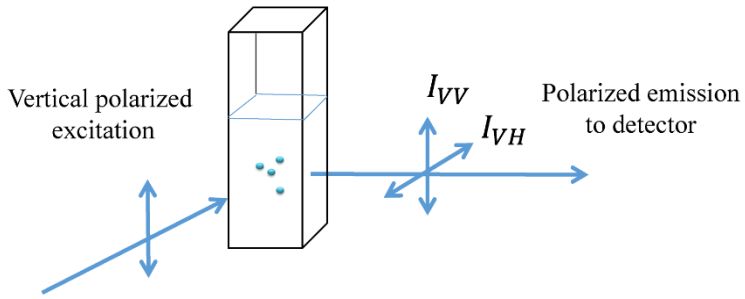


Figure 6. Schematic representation of fluorescence anisotropy detection, where $I_{XY}$ is the emitted intensity and the subscripts X and Y indicate the polarization directions of the excitation and emission light, respectively, with H and V referring to horizontal and vertical.

The anisotropy, r, is calculated from the intensities recorded with the emission polarizer arranged vertically (V) and horizontally (H), when the sample is excited with vertically polarized light. The G is the ratio of the sensitivities of the detection system for vertically and horizontally polarized light, which is measured using horizontally polarized excitation and correction factor for the instrument. See equation 7 and 8.

$$G = \frac{I_{HV}}{I_{HH}} \qquad (7)$$

$$r = \frac{I_{VV} - G\, I_{VH}}{I_{VV} + 2G I_{VH}} \qquad (8)$$

where $I_{XY}$ is the emitted intensity and the subscripts X and Y indicate the polarization directions of the excitation and emission light, respectively, with H and V referring to horizontal and vertical. When the sample is excited by linearly polarized light an average oriented excited population is generated. If the excited fluorescent molecules, fluorophores, are not allowed to move until they emit their energy the emission will be polarized as well. This property is called fundamental anisotropy ($r_0$), it depends on the angle between the absorption and emission transition dipoles, β, see equation 10.

$$r_0 = \frac{2}{5}\left(\frac{3\cos^2\beta - 1}{2}\right) \qquad (9)$$

$r_0$ can attain values between -0.2 and 0.4, corresponding to an angle of 90° and 0°, respectively, between the absorption and emission transition dipole moment.

## 3.6. Chromophores for absorbance and fluorescence assays

Different absorbance and fluorescence assays can be used to investigate enzymes behavior by spectroscopic methods, however, these assays are always based on either intrinsic protein chromophores or on an extrinsic dye which proteins are labelled with. Here, some of the assays used in this thesis are described.

### *3.6.1. Intrinsic protein assays*

Proteins can absorb the light by aromatic amino acid residues (Tyrosine and Tryptophan) and peptide bonds. However, proteins have different composition but the absorption spectrum of all proteins is characteristic with two maxima, at 200nm (peptide bonds) [46] and 280nm (aromatic residue) [45]. Many peptide bonds exist in proteins, the absorption properties of the peptide bonds at 200 nm can be used to investigate the secondary structure or the concentration of proteins. The main drawback is that many other substances used in protein solution can absorb the light in this range of wavelength such as alkenes or carbonyl compounds [46]. Therefore, to obtain a reliable data at 200 nm the proteins must be purified to make them free of any other chemicals and also the buffers should be chosen carefully. The absorption spectrum can be measured around 280 nm which is based on the aromatic amino acid, and this measurement is used for calculating the protein concentration by Beer-Lambert equation (Equation 4). Moreover, there is no limitation for using the different buffers, since the wavelength range is completely different and the buffer components

usually do not absorb the light. The amino acid composition is an important factor for the extinction coefficient of each proteins, the extinction coefficient of a protein can be determined experimentally by using solution with known concentration or based on the amino acids data composition [41, 42]. A main drawback of this method is the nucleic acids contamination that can be present in many biological samples. Since the nucleic acids can absorb the light at 260nm strongly, that can interfere the protein measurements. However, there is a possible way to calculate the protein/nucleic acid ratio and correct the nucleic acid contamination from the measurements [47] .

The intrinsic fluorescence of a folded protein is a mixture of the fluorescence from individual aromatic residues (Tryptophan and Tyrosine with the tryptophan providing the most significant portion). Mentioned before for proteins the maximum absorption is at 280 nm and an emission peak that ranges from 300 to 350 nm depending in the polarity of the local environment of the residues [45]. Fluorescence from aromatic residues gives valuable information about the structure, folding and binding interactions of proteins [45]. Since Tryptophan (Trp) is a relatively rare amino acid in proteins and has more contribution for fluorescence measurements, many studies have been aimed to investigating the fluorescence of Trp [15, 48, 49], in this case the best excitation wavelength for Trp is at 295 nm since tyrosine has very low absorption at this wavelength [50]. One advantage of intrinsic fluorescence is that a native protein can be studied with no changing in its structure, and also fluorescence studies of biomolecules in the case of particle suspensions can be useful to minimize scattering instead of using the absorbance measurements for determining the concentration [51]. The work in Paper II has been performed based on the intrinsic absorbance and fluorescence protein assay.

### *3.6.2. Extrinsic dye assays*

Since most of the interesting molecules are non-fluorescent or in some cases the intrinsic fluorescence is not proper for a desired experiment, extrinsic dyes has been discovered to label the wanted molecules since 1950s [17]. Today, many fluorophores (dyes) are available for covalent or non-covalent labelling of proteins, with longer excitation and emission wavelength compared to aromatic acids in proteins which is desirable for the proteins [45]. Some of the commercial dyes that bind proteins non-covalently or to

surfactants covering the proteins are styryl dyes (Sypro red and orange) [52], ruthenium complexes (Sypro ruby) [53]. However, some other dyes can have reaction with amino group on the protein forming fluorescent complex by covalent attachments such as SNARF-1[12] and the natural dye epicocconone [54]. The structure of epicocconone can be seen in Figure 7. The binding properties of epicocconone to a protein is discussed more in the Paper I of this thesis.

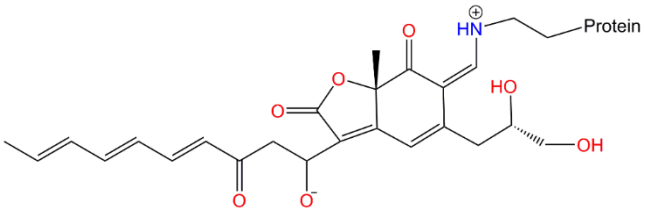


Figure 7. Structure of epicocconone bound to amino group of a protein

# 4. THEORY

## 4.1. Kinetics of enzyme immobilization in mesoporous particles

Chemical kinetics investigates how fast a process (reaction) can be completed, the rate of the process is discussed and calculated based on the data measured experimentally. Therefore, the kinetics studies can indicate how different experimental conditions can affect the speed of a reaction and more information about the reaction's mechanism. To measure the rate of a reaction the rate law is an equation that connects the reaction rate to concentrations or pressures of reactants and rate constant [55], see Equation 10:

$$r = k\,[A]^m\,[B]^n \qquad (10)$$

where A and B are the concentration of reactants, m and n are the partial reaction orders and usually are obtained experimentally, and k is the rate constant of the reaction. The value of this coefficient (k) may depend on conditions such as temperature and surface area an adsorbent.

Quantifying the kinetics of immobilization process is a crucial issue because it can be helpful for deeper understanding of the mechanism of immobilization. In immobilization process, a simple model of reaction can be assumed (Equation 11),

$$E + P \rightarrow EP \qquad (11)$$

where the protein-particle complex (EP) is the product of the reaction, and E presents free enzyme and P free binding site in the pores of the particle or on its outer surface. This model corresponds to a second-order-rate equation with rate constant k:

$$d[EP]/dt = k[E][P] \qquad (12)$$

Since in the second order reaction, the rate depends on the concentration of both reactants (here, enzymes and particles). Monitoring the concentration of two different reactants at the same time is difficult, but the reaction could be considered pseudo-first-order as a simplification, if and only if one of the reactants is used in a large excess then that concentration would hardly change at all and could be considered to be essentially a constant. If [P]>>> [E], then the [P] would be essentially unchanged and the reaction can be simplified to [56]:

$$[EP](t) = [E]_0\,(1-\exp(-k' t)) \qquad (13)$$

where $[E]_0$ is the initial concentration of protein and the pseudo first-order-rate constant ($k'$) is predicted to follow :

$$k' = k([P]_0 - [E]_0) \approx k[P]_0 \qquad (14)$$

where $[P]_0$ is the initial particle concentration and the second order rate constant k is expected to be different for each type of protein. These calculations are discussed more in the Paper I with the aim of quantifying the kinetics of immobilization process in real-time monitoring.

## 4.2. Rotational mobility of free and immobilized enzymes

The fluorescence anisotropy of a fluorophore is used to measure the protein rotational mobility on the time scale of the fluorescence lifetime. Rotational mobility can be defined as correlation rotational time (the time it takes the protein to rotate by one radian) based on Perrin equation for a protein with lifetime ($\tau$) as follows [45, 49]:

$$r = \frac{r_0}{1+\frac{\tau}{\theta}} \qquad (15)$$

where the rotational correlation time ($\theta$) is related to the steady state anisotropy ($r$) and $r_o$ is the anisotropy of the fluorophore in the absence of rotational motion. For a spherical protein with radius $R$, the rotation correlation time ($\theta$) is given by [45]

$$\theta = \frac{\eta \frac{4}{3}\pi R^3}{k\,T} \qquad (16)$$

where $\eta$ is the solution viscosity, $k$ is Boltzmann constant and $T$ the temperature.

It should be noticed that in the system of proteins immobilized in porous particles an additional process that potentially affects the anisotropy is rotation of the whole MPS particle based on Soleillet theory about depolarization [57], occurring with a rotational correlation time we denote $\theta_{part}$. To what degree each process can affect the whole system is dependent on how strong proteins are immobilized into the particles. For example, in the case of a protein which is strongly adsorbed to the pore wall the rate of rotation will be zero relative to a coordinate system fixed to the particle ($\theta_{prot} = \infty$), but the protein may still rotate as a consequence of the rotation of the particle if it is fast enough. A more detailed interpretation can be found in the Paper II for immobilization system.

## 4.3. Protein loading and pore filling

A main property of an enzyme/particle system is to know the amount of immobilized enzyme per amount of particles which usually reported as the weight of the immobilized enzyme per particle weight as called protein loading ($P_{LD}$) [1, 58]. The most common used technique for measuring the immobilized enzymes is an indirect method which is to do measurements on the solution surrounding the particles as the supernatant when the particles are sediment by centrifugation of the immobilization solution after finishing the process. However, this method cannot be suited for fast immobilization process and also for the leakage of enzyme from the particles during an enzyme-catalyzed reaction [16, 17].

As mentioned before, the protein loading is often used to show how much enzyme is adsorbed into the porous immobilization support but this cannot fully present the actual amount of protein in the pores since it depends on variation in pore volume of the particles. Therefore, a suitable parameter to describe proteins concentration in the pores is pore filling ($P_f$) which is defined as the fraction of the pore volume that is occupied by the proteins [27]:

$$P_f = V_{prot}/V_{pore} = \frac{4\pi}{3} R_H^3 N_A P_{LD}/(M_W V_{pore}) \quad (17)$$

where the volume $V_{prot}$ of (hydrated) protein is obtained from the hydrodynamic radius of protein $R_H$, protein loading ($P_{LD}$) (mass of enzyme /mass of particle), Avogadro's number and molecular weight of protein, also the $V_{pore}$ is the specific pore volume per gram of the particles which can be characterized for porous materials by Nitrogen physisorption method. To calculate the number of proteins per particle ($N_{prot}$ ) following equation can be used [27]:

$$N_{prot} = N_A \cdot P_{LD} \cdot V_{part} \cdot \rho_{part}/M_W \quad (18)$$

$V_{part}$ is the average volume per particle estimated as a sphere with diameter and $\rho_{part}$ is the density of the (dry porous) particles calculated from the particle porosity Φ as

$$\rho_{part} = \rho_{silica}(1-\Phi) = \rho_{silica}(1-V_{pore}/(V_{pore}+\rho_{silica}^{-1})) \quad (19)$$

where $\rho_{silica}$ = 2.196 g/cm$^3$ is the density of amorphous silica [27, 59].

# 5. SUMMARY OF PAPERS

This thesis is based on two papers that have been summarized in this section. The first paper suggests a fluorescence-based assay for monitoring the immobilization process in real time. The second paper describes the effect of the mesoporous particle size and the pore diameter on the rotational mobility and pore filling of immobilized enzymes.

## Paper I:

### A fluorescence spectroscopy assay for real-time monitoring of enzyme immobilization into mesoporous silica particles

This study was inspired by improving direct methods for monitoring the immobilization process, since indirect methods commonly used have low time resolution, the necessity of developing direct-monitoring methods can be recognized for studying the kinetics of enzyme immobilization in mesoporous silica particles.

Here, we investigated a fluorescence-based assay for real-time monitoring of the immobilization of lipase (MML), bovine serum albumin (BSA), and glucose oxidase (GOX) into micrometer-sized mesoporous silica particles (MPS). The proteins are labeled with the dye epicocconone (Figure 7) which is a novel extrinsic dye for measuring the concentration of enzymes which binds to amine groups of proteins forming a fluorescent product with excitation maxima at 390 and 520 nm and emission maximum is at 605 nm.

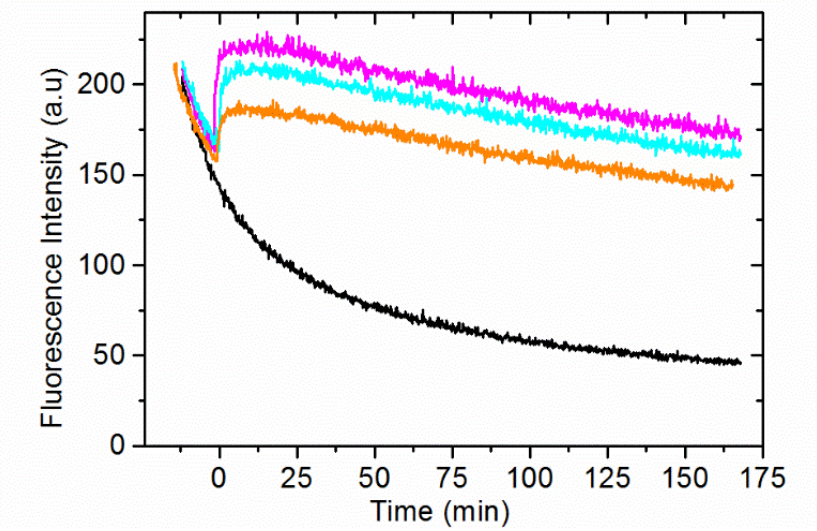


Figure 8. Raw data on the emission intensity time profiles after mixing the epicocconone–MML conjugate with the MPS particles at concentrations of 0.043 g/L (magenta, top spectrum), 0.036 g/L (cyan, second spectrum from top), 0.026 g/L (orange, third spectrum from top), and the reference conjugate sample with no particles (black, bottom spectrum). Particles were added at t = 0 min, emission wavelength: 605 nm; excitation at 520 nm.

The interaction with the particles is observed as an increase in emission intensity of the protein–dye conjugates that can be quantified if correcting for a comparatively slow photo-bleaching. The immobilization occurs in tens of minutes to hours depending on particle concentration and type of protein. In the limit of excess particles over proteins, the formation of the particle–protein complexes can be described by a single exponential growth for all three investigated proteins, and the fitted pseudo-first-order rate constant increases linearly with particle concentration for each protein type, see Figure 9.

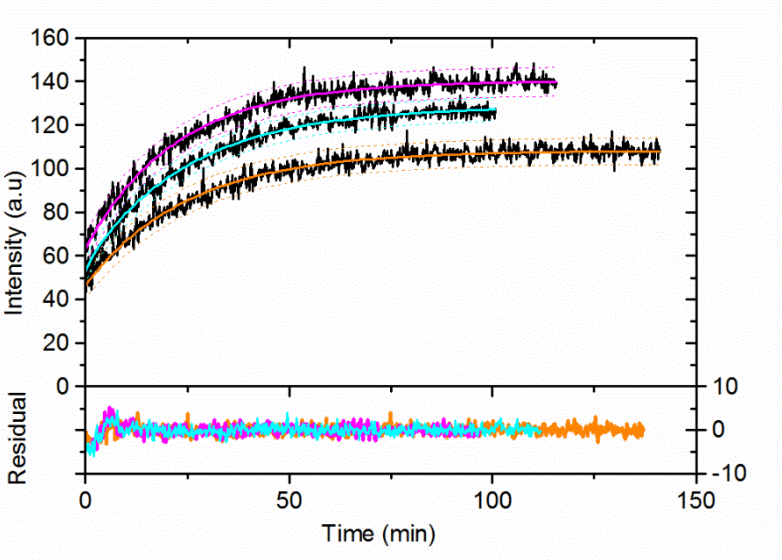


Figure 9. Bleaching-corrected emission intensity time profiles during immobilization of epicocconone–MML conjugate in the MPS particles and fitting to a single exponential growth model. Upper panel: Emission traces recorded at particle concentrations of 0.043 g/L (magenta, top spectrum), 0.036 g/L (cyan, middle spectrum), and 0.026 g/L (orange, bottom spectrum).

The full set of emission time profiles for the epicocconone conjugates with MML, BSA, and GOX in the presence of the particles at different concentrations was analyzed in the same manner. Figure 10 shows the fitted constants k´ for all three proteins plotted versus the MPS particle concentration. The results confirm that the rate constant (k´) increases with increasing particle concentrations for all three proteins.

A second order rate constant (k) for each protein was obtained from the solid line slopes in Figure 10, and the resulting values show that k decreases strongly with increasing protein size, see Figure 11. The derived second-order rate constant k varies with the protein hydrodynamic radius according to $k \sim R_H^{-4.70\pm0.01}$ which is stronger than predicted scaling. The predicted scaling ($k_d$) is $k_d \sim R_H^{-1}$ if the reaction between protein and particles is under

diffusion control. The much stronger scaling observed experimentally indicates that the immobilization at high particle concentrations is not rate controlled by diffusional encounter between protein and particles but rather the entry into the pores, consistent with the hydrodynamic radii of the three proteins being smaller but comparable to the pore radius of the particles.

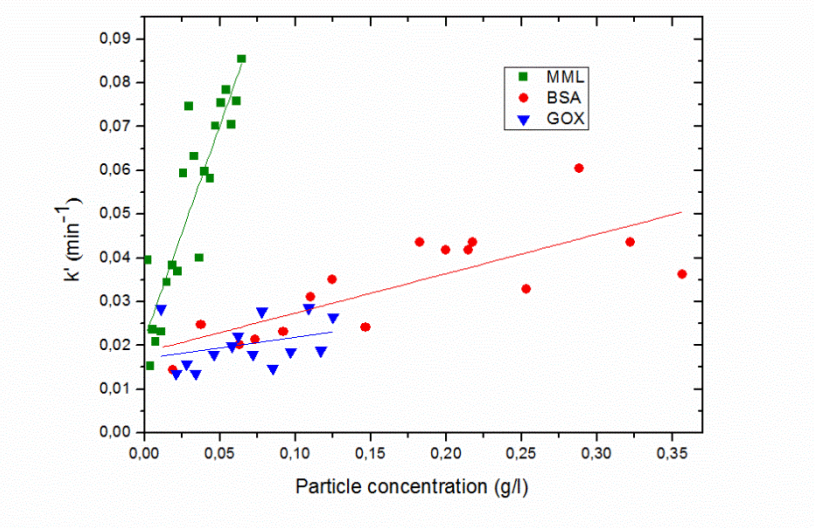


Figure 10. Pseudo-first-order rate constants k´ versus MPS particle concentration for GOX (blue inverted triangles), BSA (red circles), and MML (green squares). Solid lines are least square linear fits.

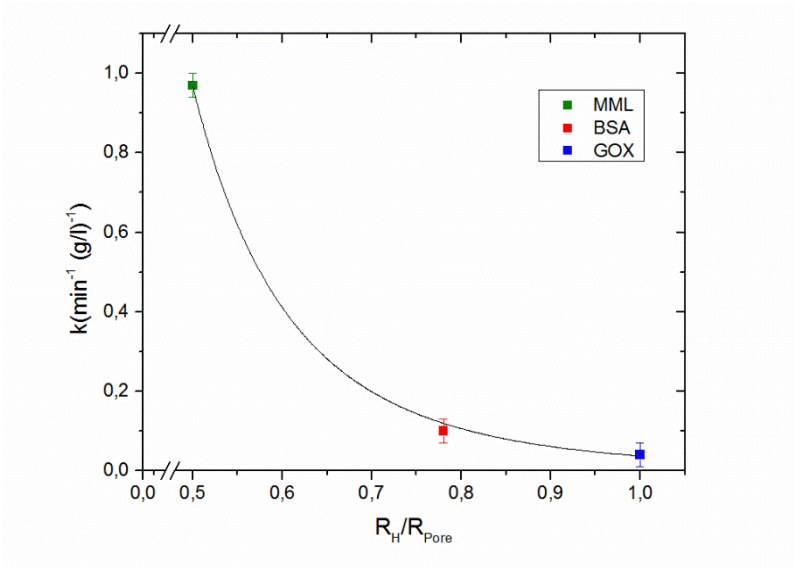


Figure 11. Plot of the second-order rate constant k versus the ratio between the hydrodynamic radii of the proteins ($R_H$) and the pore radius of the MPS particles ($R_{pore}$). The values of k are from the fitted slopes in Figure 10; error bars are from the quality of the fits.

## Paper II:

### Rotational mobility and pore filling of enzymes confined in mesoporous silica particles studied by steady state fluorescence anisotropy

Inspired by answering this scientific question that how enzyme immobilization can affect the rotational motions of enzyme in biocatalytic applications which are required to complete the catalytic activity in some reactions.

Here, we used steady state fluorescence anisotropy as a technique to investigate if immobilized proteins can rotate inside the pores more slowly than the same proteins in free solution or if the immobilized proteins are adsorbed to the pores walls which in this case are expected to rotate with the rotation rate of the particles as a single system. The proteins immobilized in different mesoporous silica particles are lipase (MML) and bovine serum albumin (BSA) which the fluorescence of their intrinsic aromatic amino acids is used for monitoring the rotational mobility of the free-solution and the immobilized proteins. Table 2 and 3 show two different conditions that are examined, first the effect of relative pore size compared to protein size and second the effect of different MPS particle dimeter and shape on rotational mobility and pore filling of the proteins.

**Table 2. Fluorescence anisotropy of free and immobilized proteins in the particles with different pore size**

| | | **MML** | | **BSA** | |
|---|---|---|---|---|---|
| **Particle type** | $R_{pore}$ [b] (nm) | r [c] | $\theta_A$ [d] (ns) | r [c] | $\theta_A$ [d] (ns) |
| Free protein [a] | ---- | 0.06 | 0.87 | 0.09 | 2.73 |
| MPS-2000 | 4.5 | 0.17 | 4.58 | 0.18 | 9.45 |
| MPS-2000 | 3.0 | 0.21 | 8.17 | 0.24 | 25.20 |

a. Protein in particle-free buffer solution.
b. Pore radius
c. Measured steady state anisotropy. The uncertainty is ±0.01 as calculated from the variation between 3 to 4 independent experiments.
d. Apparent rotational correlation time calculated from steady state anisotropy (*r*) by equation (16).The uncertainty is ±0.2 from the variation between 3 to 4 independent experiments.

In Table 2, the observed *r*-values that are intermediate between free and fully adsorbed proteins strongly indicate that the proteins do undergo some depolarizing motion inside the pores, but which is retarded compared to the free protein. This interpretation is supported by the observation that for a given protein the anisotropy is higher in the more narrow pores ($R_{pore}$: 3nm), as expected since stronger confinement is likely to change the motion more strongly. Therefore, the pore size can affect the retardation of rotational mobility of immobilized proteins.

The difference in anisotropy between different particle types in Table 3, is most likely due to their different morphology, or possibly to differences in protein-particle interaction strength. Interestingly, in MPS-300, MML exhibits the limiting anisotropy value $r_o = 0.3$, indicating essentially non-moving proteins, and BSA gives almost the same value (r = 0.27) in the same type of particle. For the other particle types in Table 3, the measured anisotropy is in an intermediate range (0.15-0.23) which is significantly lower than the upper limit $r_o = 0.3$ and again indicate that the proteins are able to rotate inside the pores, albeit more slowly than in free solution.

**Table 3. Fluorescence anisotropy of proteins immobilized in different particles types with the same pore size**

| | **MML** | | **BSA** | |
|---|---|---|---|---|
| **Particle type** [a] | r [c] | $\theta_A$ [d] (ns ) | r [c] | $\theta_A$ [d] (ns ) |
| Free protein[b] | 0.06 | 0.87 | 0.09 | 2.73 |
| MPS-40 | 0.23 | 11.5 | 0.18 | 9.45 |
| MPS-300 | 0.30 | ----- | 0.27 | 56.70 |
| MPS-1000 | 0.15 | 3.50 | 0.16 | 7.24 |
| MPS-2000 | 0.17 | 4.58 | 0.18 | 9.45 |

a. MPS-*D* where *D* is the average particle diameter in nm. The pore radius is approximately the same at 4.6+/-0.2 nm.
b. Protein in particle-free buffer solution
c. Measured tryptophan steady state anisotropy. The uncertainty is ±0.01 as calculated from the variation between 3 to 4 independent experiments.
d. Apparent rotational correlation time calculated from anisotropy by equation (16). The uncertainty is ±0.2 from the variation between 3 to 4 independent experiments.

Pore filling ($P_f$) and the number of proteins per particle ($N_{prot}$) have been calculated in each condition and based on the results the observed $P_f$ - values can decrease in smaller pore size and the values of $N_{prot}$ for all types of the MPS particles (see Figure 12) show that the larger particles accommodate many more proteins.

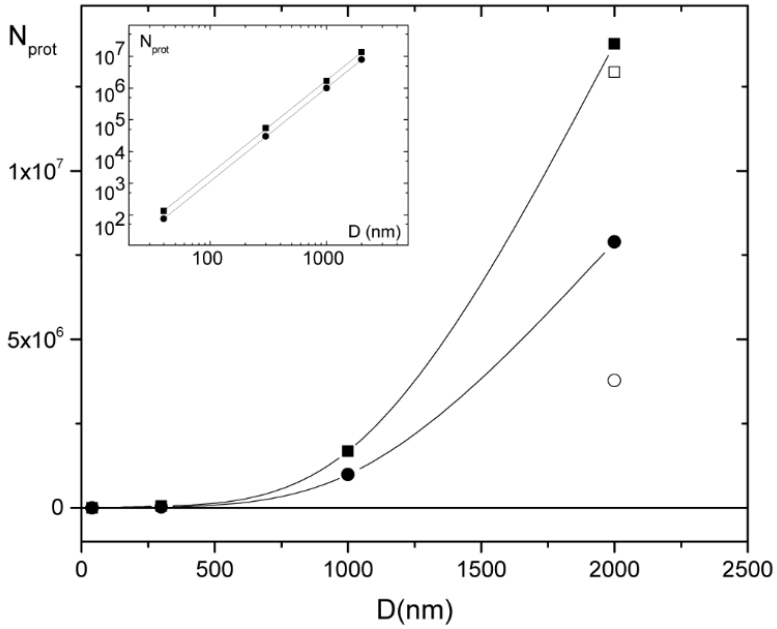


Figure 12. The average number of proteins per particle for MML (squares) and BSA (circles) versus the average particle diameter D. For pore radius 4.6+/-0.2 nm (solid; curves are guide to eye) and 3.0nm (open). Inset: Double logarithmic plot for data with 4.6 nm pore radius where straight lines are least square linear fits giving slopes 2.94+/-0.02 for MML and 2.95+/-0.01 for BSA.

In fact, the inset in Figure12 shows that the number of protein per particle (with the same pore size) scales with the linear particle size $D$ as $N_{prot} \sim D^{2.94+/-0.01}$ for MML and $N_{prot} \sim D^{2.95+/-0.01}$ for BSA. The nearly cubic scaling (i.e scaling with particle volume) supports the proposal that under our immobilization conditions both proteins essentially saturate the particle, and secondly that they are well- distributed systems. At the end three different possible mechanisms that retard the rotational mobility and pore filling are discussed which include permanent attachment of the enzymes to the pore wall, protein-protein interaction and hydrodynamic interactions with the walls.

# 6. CONCLUSION AND FUTURE PERSPECTIVE

This thesis was dedicated to the better understanding of enzymes behavior under immobilization process into solid porous silica particles and stepping forward in opening the mechanistic enigma for enzyme immobilization. Two different topics were studied. The first one, a fluorescence assay based on dye-label proteins was proposed for monitoring the kinetics of immobilization process in real time and quantifying the immobilization rate for different proteins in diameter, the larger proteins the slower immobilization rate.

In the second study, the rotational mobility of immobilized enzymes was measured by fluorescence anisotropy with no dye-labelling, the intrinsic fluorescence of aromatic amino acid residues was used for each protein. The results shows that the rate of the rotational mobility of immobilized proteins decreases compared to free protein in solution. This reduction which depends on the pore dimeter can be ascribed to three different possible mechanisms, permanent attachment of the enzymes to the pore wall, protein-protein interaction and hydrodynamic interactions with the walls.

By comparison of these studies and the analysis of the studied literature, it can be concluded that the behavior of enzymes during or after immobilization can be investigated by fluorescence spectroscopic techniques, and by choosing better probe the environment inside the pores can be better characterized. According to our knowledge, more studies are needed for fully understanding the mechanism of immobilization process.

The continuation of this project will focus in characterizing the dark (chemical) bleaching of epicocconone as the dye in the first paper and also time-resolved anisotropy studies of the second paper for achieving a fully quantitative comparison with the discussed theories in the paper which can separated the contribution of internal motion of amino acids in proteins from the global motion of enzymes.

## 7. ACKNOWLEDGEMENTS

I would like to express my gratitude to the following people:

First and foremost, my supervisor, Björn Åkerman. It is a true privilege to have you as my supervisor, for your guidance, thoughts, cares and friendship. You taught me how to think and I have learnt that solving problems takes time. *Thank you*.

My co-supervisor, Anders Palmqvist, for your precious advices and suggestions.

My examiner, Bo Albinsson, for our interesting discussions about fluorescence anisotropy.

The members of the SUPRA enzyme cluster, Lisbeth Olsson, Cyrielle Bonzom and Milene Zezzi together with Anders and Björn for nice discussions and collaborations.

Maria Abrahamsson for inviting me warmly to your Mondays group discussions and all your guidance in science and non-science.

My co-authors, Nils and Kassam, for all your effort.

My dear officemates, Rita, Kubra, Damir and Amir for all laughs, nicknames and secrets!!

My wonderful friends, Mehrnaz and Hoda for all the beautiful moments and all your helps. And Nerine for your encouragements.

Mahna for being my best friend forever and all *laughter and tears*.

Shaghayegh and Elham, side by side or miles apart, sisters are always joined heart to heart. *Thank you*.

My lovely parents, Pooran and Seyed Ebrahim for your endless love and support in all my life.

And my bestie, Sam, for being always on my side no matter what and definitely your *love*.

# 8. BIBLIOGRAPHY

1. Lee, C.-H., T.-S. Lin, and C.-Y. Mou, *Mesoporous materials for encapsulating enzymes.* Nano Today, 2009. **4**(2): p. 165-179.
2. Lei, C.H., et al., *Entrapping enzyme in a functionalized nanoporous support.* Journal of the American Chemical Society, 2002. **124**(38): p. 11242-11243.
3. Lei, C.H., et al., *Enzyme specific activity in functionalized nanoporous supports.* Nanotechnology, 2008. **19**(12): p. 9.
4. Hudson, S., et al., *Methodology for the immobilization of enzymes onto mesoporous materials.* Journal of Physical Chemistry B, 2005. **109**(41): p. 19496-19506.
5. Giraldo, L.F., et al., *Mesoporous Silica Applications.* Macromolecular Symposia, 2007. **258**(1): p. 129-141.
6. Miyahara, M., A. Vinu, and K. Ariga, *Adsorption myoglobin over mesoporous silica molecular sieves: Pore size effect and pore-filling model.* Materials Science and Engineering: C, 2007. **27**(2): p. 232-236.
7. Hudson, S., J. Cooney, and E. Magner, *Proteins in Mesoporous Silicates.* Angewandte Chemie-International Edition, 2008. **47**(45): p. 8582-8594.
8. Wang, X., et al., *Enzyme-Nanoporous Gold Biocomposite: Excellent Biocatalyst with Improved Biocatalytic Performance and Stability.* Plos One, 2011. **6**(9).
9. Andersson, N., et al., *Structural features and adsorption behaviour of mesoporous silica particles formed from droplets generated in a spraying chamber.* Microporous and Mesoporous Materials, 2004. **72**(1–3): p. 175-183.
10. B. Massey, J. and J.E. Churchich, *Nanosecond spectroscopy of a dimeric enzyme: plasma amine oxidase.* Biophysical Chemistry, 1979. **9**(2): p. 157-162.
11. Thörn, C., H. Gustafsson, and L. Olsson, *Immobilization of feruloyl esterases in mesoporous materials leads to improved transesterification yield.* Journal of Molecular Catalysis B: Enzymatic, 2011. **72**(1–2): p. 57-64.
12. Thörn, C., et al., *A method to measure pH inside mesoporous particles using protein-bound SNARF1 fluorescent probe.* Microporous and Mesoporous Materials, 2013. **165**: p. 240-246.
13. Yamaguchi, A., et al., *Acid-base equilibria inside amine-functionalized mesoporous silica.* Anal Chem, 2011. **83**(8): p. 2939-46.
14. Ingersoll, C.M. and C.M. Strollo, *Steady-State Fluorescence Anisotropy To Investigate Flavonoids Binding to Proteins.* Journal of Chemical Education, 2007. **84**(8): p. 1313.
15. Lakowicz, J.R., G. Freshwater, and G. Weber, *Nanosecond segmental mobilities of tryptophan residues in proteins observed by lifetime-resolved fluorescence anisotropies.* Biophys J, 1980. **32**(1): p. 591-601.
16. Bradford, M.M., *A rapid and sensitive method for the quantitation of microgram quantities of protein utilizing the principle of protein-dye binding.* Anal Biochem, 1976. **72**: p. 248-54.
17. Lowry, O.H., et al., *Protein measurement with the Folin phenol reagent.* J Biol Chem, 1951. **193**(1): p. 265-75.
18. Nishimoto, E., et al., *Internal motion of lysozyme studied by time-resolved fluorescence depolarization of tryptophan residues.* Biochemistry, 1998. **37**(16): p. 5599-607.
19. Lehninger, A., D. Nelson, and M. Cox, *Lehninger Principles of Biochemistry*. 2008: W. H. Freeman.
20. Berg, J.M., J.L. Tymoczko, and L. Stryer, *Biochemistry*. 2002: W.H. Freeman.
21. Kirk, O., T.V. Borchert, and C.C. Fuglsang, *Industrial enzyme applications.* Curr Opin Biotechnol, 2002. **13**(4): p. 345-51.

22. Gustafsson, H., C. Thörn, and K. Holmberg, *A comparison of lipase and trypsin encapsulated in mesoporous materials with varying pore sizes and pH conditions.* Colloids and Surfaces B: Biointerfaces, 2011. **87**(2): p. 464-471.
23. Zoldak, G., et al., *Irreversible thermal denaturation of glucose oxidase from Aspergillus niger is the transition to the denatured state with residual structure.* J Biol Chem, 2004. **279**(46): p. 47601-9.
24. Ge, S., et al., *Bovine serum albumin adsorption onto immobilized organotrichlorosilane surface: influence of the phase separation on protein adsorption patterns.* J Biomater Sci Polym Ed, 1998. **9**(2): p. 131-50.
25. Hirayama, K., et al., *Rapid confirmation and revision of the primary structure of bovine serum albumin by ESIMS and Frit-FAB LC/MS.* Biochem Biophys Res Commun, 1990. **173**(2): p. 639-46.
26. Yang, P., et al., *Generalized syntheses of large-pore mesoporous metal oxides with semicrystalline frameworks.* Nature, 1998. **396**(6707): p. 152-155.
27. Carlsson, N., et al., *Enzymes immobilized in mesoporous silica: A physical–chemical perspective.* Advances in Colloid and Interface Science, (0).
28. Deng, W., et al., *Characterization of mesoporous alumina molecular sieves synthesized by nonionic templating.* Microporous and Mesoporous Materials, 2002. **52**(3): p. 169-177.
29. Antonelli, D.M. and J.Y. Ying, *Synthesis of Hexagonally Packed Mesoporous TiO2 by a Modified Sol–Gel Method.* Angewandte Chemie International Edition in English, 1995. **34**(18): p. 2014-2017.
30. Gustafsson, H., et al., *Immobilization of lipase from Mucor miehei and Rhizopus oryzae into mesoporous silica—The effect of varied particle size and morphology.* Colloids and Surfaces B: Biointerfaces, 2012. **100**(0): p. 22-30.
31. Zhao, D.Y., et al., *Triblock copolymer syntheses of mesoporous silica with periodic 50 to 300 angstrom pores.* Science, 1998. **279**(5350): p. 548-552.
32. Zhao, D.Y., et al., *Nonionic triblock and star diblock copolymer and oligomeric surfactant syntheses of highly ordered, hydrothermally stable, mesoporous silica structures.* Journal of the American Chemical Society, 1998. **120**(24): p. 6024-6036.
33. Robens, E., *Adsorption by powders and porous solids. F. Rouquerol, J. Rouquerol, K. Sing, Academic Press, San Diego 1999, ISBN: 0-12-598920-2, 467 S. £79.95.* Vakuum in Forschung und Praxis, 1999. **11**(3): p. 191-191.
34. Stein, A., B.J. Melde, and R.C. Schroden, *Hybrid Inorganic–Organic Mesoporous Silicates—Nanoscopic Reactors Coming of Age.* Advanced Materials, 2000. **12**(19): p. 1403-1419.
35. Li, L.-L., et al., *Optical sensors based on functionalized mesoporous silica SBA-15 for the detection of multianalytes (H+ and Cu2+) in water.* Journal of Materials Chemistry, 2007. **17**(42): p. 4492-4498.
36. Melde, B., B. Johnson, and P. Charles, *Mesoporous Silicate Materials in Sensing.* Sensors, 2008. **8**(8): p. 5202.
37. Hecht, E., *Optics (4th Edition)*. 2001: Addison Wesley.
38. Broglie, L.d., *XXXV. A tentative theory of light quanta.* Philosophical Magazine Series 6, 1924. **47**(278): p. 446-458.
39. Bohr, N., *I. On the constitution of atoms and molecules.* Philosophical Magazine Series 6, 1913. **26**(151): p. 1-25.
40. Swinehart, D.F., *The Beer-Lambert Law.* Journal of Chemical Education, 1962. **39**(7): p. 333.
41. Gill, S.C. and P.H. von Hippel, *Calculation of protein extinction coefficients from amino acid sequence data.* Anal Biochem, 1989. **182**(2): p. 319-26.

42. Pace, C.N., et al., *How to measure and predict the molar absorption coefficient of a protein.* Protein Sci, 1995. **4**(11): p. 2411-23.
43. Mie, G., *Beiträge zur Optik trüber Medien, speziell kolloidaler Metallösungen.* Annalen der Physik, 1908. **330**(3): p. 377-445.
44. Strutt, J.W., *LVIII. On the scattering of light by small particles.* Philosophical Magazine Series 4, 1871. **41**(275): p. 447-454.
45. Lakowicz, J.R., *Principles of Fluorescence Spectroscopy*. 3rd ed. 2006, Baltimor, USA: Springer.
46. Goldfarb, A.R., *Absorption spectrum of the peptide bond. II. Influence of chain length.* J Biol Chem, 1953. **201**(1): p. 317-20.
47. Warburg, O. and W. Christian, *Insulation and Crystalisation of the Fermenting Process of Enolase.* Biochem Z, 1942. **310**(6): p. 384 - 421.
48. Graupner, M., et al., *Molecular Dynamics of Microbial Lipases as Determined from Their Intrinsic Tryptophan Fluorescence.* Biophysical Journal, 1999. **77**(1): p. 493-504.
49. Lakowicz, J.R., et al., *Rotational freedom of tryptophan residues in proteins and peptides.* Biochemistry, 1983. **22**(8): p. 1741-1752.
50. Albrecht, C., *Joseph R. Lakowicz: Principles of fluorescence spectroscopy, 3rd Edition.* Analytical and Bioanalytical Chemistry, 2008. **390**(5): p. 1223-1224.
51. Nabavi Zadeh, P.S., et al., *A fluorescence spectroscopy assay for real-time monitoring of enzyme immobilization into mesoporous silica particles.* Analytical Biochemistry, 2015. **476**: p. 51-58.
52. Zubkov, M.V., et al., *Determination of total protein content of bacterial cells by SYPRO staining and flow cytometry.* Appl Environ Microbiol, 1999. **65**(7): p. 3251-7.
53. Berggren, K., et al., *A luminescent ruthenium complex for ultrasensitive detection of proteins immobilized on membrane supports.* Anal Biochem, 1999. **276**(2): p. 129-43.
54. Bell, P.J.L. and P. Karuso, *Epicocconone, A Novel Fluorescent Compound from the Fungus Epicoccum nigrum.* Journal of the American Chemical Society, 2003. **125**(31): p. 9304-9305.
55. Atkins, P. and J. de Paula, *Atkins' Physical Chemistry*. 2010: OUP Oxford.
56. Atkins, P., J. de Paula, and R. Friedman, *Quanta, Matter, and Change: A Molecular Approach to Physical Change*. 2008: W. H. Freeman.
57. Soleillet, P., *Sur les parametres caractérisant la polarisation partielle de la lumiere dans les phénomenes de fluorescence*. Ann.Phys.Biol.Med. 1929: Ann.Phys.Biol.Med.
58. Lei, C., et al., *Characterization of functionalized nanoporous supports for protein confinement.* Nanotechnology, 2006. **17**(22): p. 5531-8.
59. Haynes, W.M. and D.R. Lide, *CRC handbook of chemistry and physics : a ready-reference book of chemical and physical data*. 2011, Boca Raton, Fla.: CRC Press.

***Paper I***

Analytical Biochemistry 476 (2015) 51–58

Contents lists available at ScienceDirect

Analytical Biochemistry

journal homepage: www.elsevier.com/locate/yabio

# A fluorescence spectroscopy assay for real-time monitoring of enzyme immobilization into mesoporous silica particles

Pegah S. Nabavi Zadeh, Kassam Abdel Mallak, Nils Carlsson [1], Björn Åkerman *

*Department of Chemistry and Chemical Engineering, Physical Chemistry, Chalmers University of Technology, SE-412 96 Gothenburg, Sweden*

ARTICLE INFO

*Article history:*
Received 22 December 2014
Received in revised form 3 February 2015
Accepted 3 February 2015
Available online 11 February 2015

*Keywords:*
Enzyme
Immobilization
Mesoporous silica
Kinetics
Fluorescence
Epicocconone

ABSTRACT

Mesoporous silica particles are used as support material for immobilization of enzymes. Here we investigated a fluorescence-based assay for real-time monitoring of the immobilization of lipase, bovine serum albumin, and glucose oxidase into micrometer-sized mesoporous silica particles. The proteins are labeled with the dye epicocconone, and the interaction with the particles is observed as an increase in emission intensity of the protein–dye conjugates that can be quantified if correcting for a comparatively slow photobleaching. The immobilization occurs in tens of minutes to hours depending on particle concentration and type of protein. In the limit of excess particles over proteins, the formation of the particle–protein complexes can be described by a single exponential growth for all three investigated proteins, and the fitted pseudo-first-order rate constant increases linearly with particle concentration for each protein type. The derived second-order rate constant $k$ varies with the protein hydrodynamic radius according to $k \sim R_H^{-4.70\pm0.01}$, indicating that the rate-limiting step at high particle concentrations is not the diffusional encounter between proteins and particles but rather the entry into the pores, consistent with the hydrodynamic radii of the three proteins being smaller but comparable to the pore radius of the particles.


Immobilization of enzymes into mesoporous silica particles is an intense area of research mainly because of the biocatalyst applications, but it is also of interest in biosensing, biofuels, and controlled drug release [1,2]. Enzymes are effective and useful biocatalysts with high selectivity, but the use of free enzymes often leads to difficulties in the separation of product and enzyme as well as high costs and low protein stability [3,4]. Enzyme immobilization into a solid support is a method developed to minimize the effects of these limitations, and a common support material is mesoporous silica due to advantageous properties such as a large surface area, a narrow pore size distribution, and high chemical and thermal stability. Immobilized enzymes sometimes also tolerate more extreme pH, elevated temperature, and higher salt concentration than the same protein in bulk solution [5].

The most frequently used approach for monitoring the immobilization process is to study the solution surrounding the particles through measurements on the supernatant after the protein particle suspension has been subjected to centrifugation. This technique is used to determine the amount of encapsulated protein (reviewed in Ref. [5]) and sometimes also to monitor the kinetics of the immobilization [6]. A drawback often inherent in such indirect methods is high uncertainty and low sensitivity, and another limitation is the low time resolution that results from the time-consuming protocols for measuring protein concentration in bulk solution such as the Bradford method [7]. A few recent studies have introduced biophysical methods that allow for the direct monitoring of the immobilization process [5]. For example, quartz crystal microbalance with dissipation monitoring (QCM-D)[2] has been reported as a method for studying enzyme immobilization in mesoporous silica particles in real time [8]. The QCM-D measurements show that more enzymes are immobilized into mesoporous silica particles than into nonporous particles and onto a flat silica surface, directly confirming the protein uptake into the pores. In the QCM-D approach, protein binding was monitored through the effects on the mass and viscoelastic properties of a film of mesoporous silica particles adsorbed to a macroscopic surface. Therefore, it would be interesting to develop a direct method that can be used with particle suspensions because this is the most common encapsulation format in applications of enzyme immobilization.

* Corresponding author.
*E-mail address:* baa@chalmers.se (B. Åkerman).
[1] Current address: Borealis, SE-444 86 Stenungsund, Sweden.

[2] *Abbreviations used:* QCM-D, quartz crystal microbalance with dissipation monitoring; UV–vis, ultraviolet–visible; BSA, bovine serum albumin; MML, *Mucor miehei* lipase; GOX, glucose oxidase; MPS, mesoporous silica; DOI, degree of immobilization.

http://dx.doi.org/10.1016/j.ab.2015.02.005
0003-2697/

Ultraviolet–visible (UV–vis) spectroscopy is often used to study proteins in solution regarding fundamental properties such as tertiary structure using circular dichroism [9] and protein concentration using visible absorption [7], exploiting either native chromophores such as tryptophan amino acid residues or dye labels attached to the proteins such as bromophenol blue. Spectroscopic studies of biomolecules in the case of particle suspensions is commonly hampered in the UV–vis range by the turbidity stemming from particle light scattering, but one approach to minimize scattering effects is to use fluorescence that is less sensitive to turbidity than absorption spectroscopy. In this approach, the proteins generally need to be labeled with a fluorescent dye because the autofluorescence of native proteins is too weak with a few exceptions such as green fluorescent protein [10,11]. Fluorescence spectroscopy has been used, for example, to measure the pH sensed by proteins immobilized inside silica particles [12,13]. In one approach, a pH-sensitive probe was attached to the silica walls of the particle pores and interrogated by fluorescence spectroscopy [13]. In a reverse approach, the pH-sensitive fluorescent probe SNARF-1 was attached covalently to the proteins [12] with the aim that the recorded emission spectrum reflected the pH at the actual location of the encapsulated proteins. Similarly, Matsuura and coworkers [14] used labeled proteins and fluorescence energy transfer spectroscopy to investigate how pore size affects protein distances in a silica-based mesoporous material. Importantly, at least for the proteins (bovine serum albumin [BSA] and a feruloyl esterase) studied in the SNARF-1 investigation [12], the dye had no detectable effect on the protein structure, degree of immobilization, or enzymatic activity. These results show how spectroscopic probes carried by immobilized proteins can be used to characterize the environment and interactions between proteins, once they are immobilized inside mesoporous particles, without perturbing the properties of the materials.

The spectroscopic studies [3,5,15] have often been aimed at the ultimate outcome of the encapsulation such as how the enzymes are affected by the environment in the pores or how the immobilized enzymes are distributed inside the porous particles. Here we investigated whether a spectroscopy approach can be used to monitor the whole immobilization process in real time starting with the mixing of the proteins and particles. Our main aim was to quantify the kinetics of the immobilization because a deeper understanding of the mechanistic steps of enzyme transport into the pores of the silica particles is needed to improve the encapsulation efficiency in the various applications. Here we propose a fluorescence spectroscopy assay based on dye-labeled proteins and use it to measure how the rate of immobilization depends on protein size for a given pore size. To this end, lipase, BSA, and glucose oxidase were labeled covalently with the fluorescent dye epicocconone, commonly used for protein concentration determination in bulk solution. The hydrodynamic radii of these proteins (2.25, 3.5, and 4.5 nm) are smaller than but comparable to the pore radius of the particles (4.6 nm) and are much smaller than the average particle diameter (1 μm). The degree of immobilization at the end of the process is also estimated by fluorescence spectroscopy, but quantifying the kinetics of immobilization was the focus of the study.

## Materials and methods

### Chemicals and particles

Lipase (*Mucor miehei* lipase, MML), albumin (BSA), and glucose oxidase (GOX from *Aspergillus niger*) were obtained from Sigma–Aldrich. Epicocconone was obtained from Sigma–Aldrich as part of the FluoroProfile Kit for protein quantification. The mesoporous silica (MPS) particles of SBA-15 type were a gift from Hanna Gustafsson (Applied Chemistry, Chalmers University of Technology) [16,17] and were synthesized and characterized as described previously [16–18]. Briefly, nitrogen adsorption isotherms gave an average pore diameter of 9.3 nm, a specific pore volume of 1.18 $cm^3/g$, and a BET (Brunauer–Emmett–Teller) surface area of 502 $m^2/g$ [16,17]. According to transmission electron microscopy, the pores are hexagonally shaped with a radius of 4.6 nm and an average diameter of the particles of 1 μm. All experiments were performed at 25 °C and in 0.1 M phosphate citrate buffer to give pH 6.0 if not otherwise stated.

### Binding of epicocconone to proteins

Epicocconone (Fig. 1) binds to amine groups of proteins, forming a fluorescent product [22] with excitation maxima at 390 and 520 nm and an emission maximum at 605 nm [23]. The dye modification of the proteins was performed by mixing 400 μl of protein–buffer solutions (2 mg protein/ml and 0.1 M phosphate citrate buffer, pH 8.0) with a mixture of 250 μl epicocconone reagent and 350 μl quantification buffer, both provided in the FluoroProfile Kit. After 1 h of incubation, the labeled protein (violet) was purified on a size exclusion column (NAP-10, GE Healthcare) in 0.1 M phosphate citrate buffer (pH 8.0) to remove all nonbound epicocconone. The number of attached epicocconone per protein (the degree of labeling [DOL] in Table 1) was determined based on the absorbance ratio of the dye ($A_{520\ nm}$) and the proteins ($A_{280\ nm}$) before and after the binding reaction [12] using the molar extinction coefficient ($\varepsilon_{520}$) 11,200 $M^{-1}\ cm^{-1}$ at 520 nm for epicocconone and the protein molar extinction coefficients at 280 nm ($\varepsilon_{280}$) given in Table 1.

### Particle solutions

Working solutions of MPS (5–14 g/L) were prepared by suspending the required mass of dry MPS particles in phosphate citrate

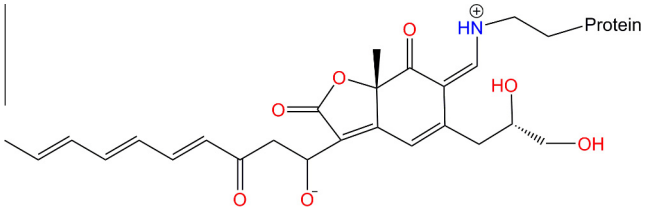


**Fig.1.** Epicocconone bound to amine group of a protein.

**Table 1**
Properties and results for the proteins.

| Protein[a] | $M_w$[b] (kDa) | $R_H$[c] (nm) | p$I$[d] | $\varepsilon_{280}$[e] ($M^{-1}\ cm^{-1}$) | DOL[f] | $k$[g] [(g/L)$^{-1}$ min$^{-1}$] |
|---|---|---|---|---|---|---|
| MML | 32 | 2.25 | 3.8 | 42,800 | 1.6 | 0.97 ± 0.02 |
| BSA | 66 | 3.5 | 4.7 | 43,824 | 8.3 | 0.09 ± 0.02 |
| GOX | 160 | 4.5 | 4.2 | 308,000 | 1.9 | 0.04 ± 0.02 |

[a] MML, *Mucor miehei* lipase; BSA, bovine serum albumin; GOX, glucose oxidase.
[b] Molecular mass [6,19,20].
[c] Hydrodynamic radius [6,12,20].
[d] Isoelectric point [6,12,20].
[e] Extinction coefficient at 280 nm [6,12,21].
[f] Degree of labeling (epicocconone per protein).
[g] Second-order rate constant $k$ from linear fits in Fig. 5 with errors corresponding to the uncertainties in the fits.

buffer at pH 6.0 using vortexing for 10 min at 10 rpm followed by sonication (Ultrasonic cleaner model CD-4800 at 70 W power) for 30 min to dissolve any particle aggregates and then a second step of vortexing. The vortexing and sonication procedure was repeated before aliquots were removed for the preparation of the particle–protein samples.

### *Spectroscopic measurements*

Emission spectra (520–800 nm) were recorded on a Cary Eclipse fluorimeter (Varian) with excitation at 520 nm and with excitation and emission slit widths at 20 nm. All fluorescence measurements were performed with emission detected at 90° to the excitation light beam. For the real-time monitoring of kinetics, the fluorimeter was equipped with four cuvettes that were monitored in parallel using an emission wavelength of 605 nm (peak in the emission spectra) with excitation at 520 nm.

### *Protein immobilization and data analysis*

The immobilization was performed by using established protocols [12] for dye-modified proteins that are known to give a degree of immobilization (DOI) in the MPS particles that is the same as for the nonlabeled form of the proteins. For the kinetic studies, the four cuvettes initially contained 2.5 ml of the same sample of labeled protein with a concentration $4.5 \times 10^{-8}$ M protein in citrate–phosphate buffer at pH 6.0 and a small bar magnet to stir the samples continuously during the spectroscopic measurements to prevent particle sedimentation. After 10 min of equilibration, the small samples of the MPS working solution, typically (20–50 µl), were added to three of the cuvettes, giving three different final particle concentrations between 0.0018 and 0.360 g/L. The fourth cuvette was kept as a particle-free reference to monitor bleaching of the dye during the spectroscopic measurements of the immobilization process, which lasted up to 3 h depending on the MPS particle concentration. The kinetic experiments were repeated three times for each combination of particle concentration and protein type (keeping protein concentration at $4.5 \times 10^{-8}$ M). The recorded emission time profiles of the samples at 605 nm were corrected for photochemical bleaching of the protein–dye conjugate by subtracting the corresponding intensity profile of the particle-free reference sample (see Results), thereby making the assumption that the bleaching processes are not affected by the presence of the particles. Our results show that part of the bleaching is due to a non-light-dependent reaction, so it was not possible to avoid the bleaching by incubation in the dark.

The resulting intensity profiles $I(t)$ were fitted to a single exponential growth function,

$$I = I_o + A(1 - e^{k't}), \quad (1)$$

where $I_o$ is the intensity before the particles are added (defined as $t = 0$) and $k'$ is a (pseudo-first-order) rate constant. In Eq. (1), the intensity $I_o$ and the pre-exponential factor $A$ will depend on the degree of dye labeling of the protein (Table 1) and the quantum yield of the free and immobilized protein–dye conjugate (see Online supplementary material).

The DOI at the end of the incubation was estimated from the emission intensity of the supernatant ($I_{sup}$) at 605 nm after the particles had been removed by centrifugation. The fraction ($f_{DOI}$) of immobilized proteins was calculated as $f_{DOI} = 1 - I_{sup}/I_{bs}$, where $I_{bs}$ is the intensity at 605 nm of the sample just before the particles were spun down, to take into account the epicocconone bleaching that occurs during the incubation.

## Results

### *Effect of MPS particles on emission spectra of epicocconone–protein conjugates*

Fluorescence emission spectroscopy of MML, BSA, and GOX was used to investigate the interaction between the proteins and the MPS particles (pore radius of $R_{pore} = 4.6$ nm). In Fig. 2, curve a shows the emission spectrum of the epicocconone–MML conjugate without the MPS particles and curve b shows the spectrum of the same sample after the labeled proteins had been incubated with the MPS particles for 180 min. It is seen that the emission intensity has decreased after the incubation but that the shape of the spectrum is essentially unaffected with an emission maximum at 603 nm. If the same epicocconone–MML sample was incubated without particles for the same amount of time under identical conditions (curve c), the spectral shape is still the same but the intensity is even lower.

The type of changes in the emission spectrum we observe when the MPS particles are mixed with MML were also seen with the epicocconone conjugates of the two other proteins (see Fig. S-1 in Supplementary material). Here we exploit that the intensity is higher in the presence of the particles to monitor the immobilization process in real time.

### *Fluorescence monitoring of immobilization kinetics*

The interactions between all three labeled proteins and the MPS particles were monitored in real time by measuring the emission intensity versus time at the wavelength 605 nm of maximum emission (Fig. 2). In Fig. 3, the three upper curves show the emission time profiles for the epicocconone–MML conjugate after particles were added at $t = 0$ min to give three different MPS concentrations. The lower curve shows the intensity time profile for the reference sample (no particles) when it is subject to the same illumination as the samples containing particles. It is seen that the reference sample exhibits a steady decrease in intensity during the illumination, and control experiments with intermittent illumination (see "Bleaching mechanism" section below) shows that this decline is due to photobleaching of the protein-bound dye because of the long illumination, in combination with a dark reaction that also reduces the quantum yield of the dye. By contrast, the protein samples containing particles first exhibit an

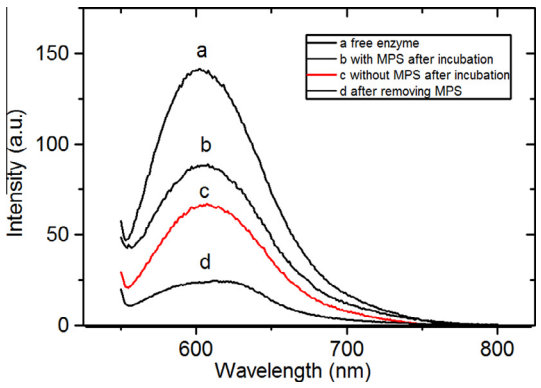


**Fig.2.** Emission spectra of epicocconone–MML conjugate: (a) free enzyme before the particles have been added; (b) after incubation with MPS for 180 min; (c) after 180 min without MPS; (d) of the supernatant after the particles in the sample of curve b have been removed by centrifugation. Excitation wavelength: 520 nm; particle concentration: 0.055 g/L; protein concentration: $4.5 \times 10^{-8}$ M. During incubation of curves b and c, the samples were exposed to the same continuous illumination.

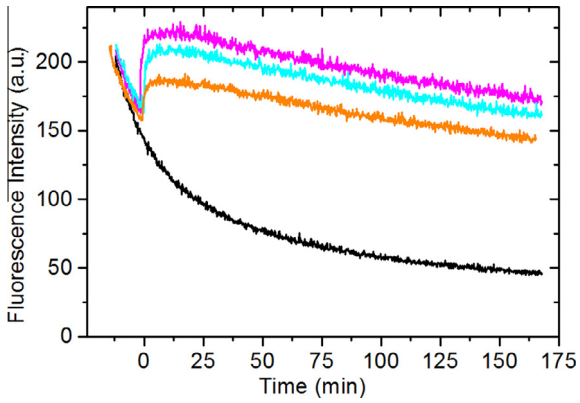


**Fig.3.** Raw data on the emission intensity time profiles after mixing the epicocconone–MML conjugate with the MPS particles at concentrations of 0.043 g/L (magenta, top spectrum), 0.036 g/L (cyan, second spectrum from top), 0.026 g/L (orange, third spectrum from top), and the reference conjugate sample with no particles (black, bottom spectrum). Particles were added at $t = 0$ min. Protein concentration: $4.5 \times 10^{-8}$ M; emission wavelength: 605 nm; excitation at 520 nm. (For interpretation of the references to colour in this figure legend, the reader is referred to the web version of this article.)

increase in intensity when the particles are added before a similar decline in intensity is observed at longer times.

The observed increase in intensity just after adding the particles indicates that the epicocconone fluorescence increases when the labeled proteins interact with the MPS particles, which is the actual effect we exploited to monitor the immobilization process.

The intensity profiles in Fig. 3 are all lower than the initial value after 180 min, which is in agreement with the spectra in Fig. 2 because spectrum b has lower intensity than the initial spectrum a at the end of the incubation. However, in the absence of particles, the final spectrum c is even lower than spectrum b because the bottom curve of Fig. 3 lacks the initial increase in intensity seen in the samples with particles present. The protein binding to the particles, therefore, can be detected as an increase in intensity even though there is a net decrease in intensity at the end of the incubation.

In Fig. 2, curve d shows the emission spectrum of the supernatant of the MML sample in curve b after the particles have been removed by centrifugation and, thus, corresponds to the proteins that remain in the surrounding solution after 180 min of incubation. The remaining intensity corresponds to the fact that approximately 72% of the added protein has been immobilized as calculated from the relative decrease in intensity at the wavelength of maximum emission (see Materials and Methods above).

The same type of behavior shown in Fig. 3 was observed when the same experiment was performed with different MPS concentrations between 0.0018 and 0.360 g/L and when BSA or GOX was used instead of MML (results not shown). Only in the case of GOX was there a qualitatively different behavior at MPS particle concentrations above 0.14 g/L because the intensity exhibited a fast sharp peak after the addition of particles typically lasting a few minutes (see Fig. S-2 in Supplementary material), which was followed by the same rise and decay pattern seen in the MPS particle samples in Fig. 3. The kinetic data collection for GOX, therefore, was limited to particle concentrations below 0.14 g/L. The DOI of GOX and BSA were comparable to MML at 83 and 75%, respectively. These representative DOI values show that a major fraction of the added protein ultimately becomes bound to the particles under our conditions (in the pores or on the external surface), so the kinetic results in Fig. 3 indeed reflect the rate of immobilization.

*Data analysis and rate constants*

The intensity data of the protein–particle samples in Fig. 3 were corrected for the long-term bleaching of the dye by subtracting the concurrent reference data on proteins without particles, which were recorded in the same fluorescence experiment to ensure the same illumination conditions. Fig. 4 shows the corrected time profiles obtained in this manner for MML at three different particle concentrations using the data in Fig. 3. In the upper panel of Fig. 4, the black curves show the corrected data and the solid lines are the fits to single exponential growth (Eq. (1)). The lower panel of Fig. 4 shows the residuals between the bleaching-corrected experimental data and the exponential fits. The single exponential growth model is seen to describe the experimental data well except during the first 20 min, where a small peak in the residual indicates the presence of a fast but weak component in the intensity growth. The values of the kinetic constant $k'$ (see Eq. (1)) obtained from the fits in Fig. 4 (0.10, 0.09, and 0.07 $\text{min}^{-1}$ for 0.043, 0.036, and 0.026 g/L MPS, respectively) show that a higher MPS concentration leads to a faster interaction with the proteins.

The full set of emission time profiles for the epicocconone conjugates with MML, BSA, and GOX in the presence of the particles at different concentrations was analyzed in the same manner. Fig. 5 shows the fitted constants $k'$ for all three proteins plotted versus the MPS particle concentration. In spite of some scattering in the data, the results confirm that the rate constant ($k'$) increases with increasing particle concentrations for all three proteins. A second-order rate constant ($k$) for each protein was obtained from the solid line slopes in Fig. 5, and the resulting values (see Table 1) show that $k$ decreases strongly with increasing protein size.

*Spectroscopic properties of epicocconone–protein conjugates*

Fig. 6 compares the normalized emission spectra of epicocconone dye when bound to the three proteins before they were immobilized in the MPS particles. The spectra with GOX and BSA both have a maximum at 605 nm and are essentially superimposable, indicating that the dye is bound in the same way to the two proteins and in a similar local environment on the protein surface. The emission spectrum for the epicocconone–MML conjugate is

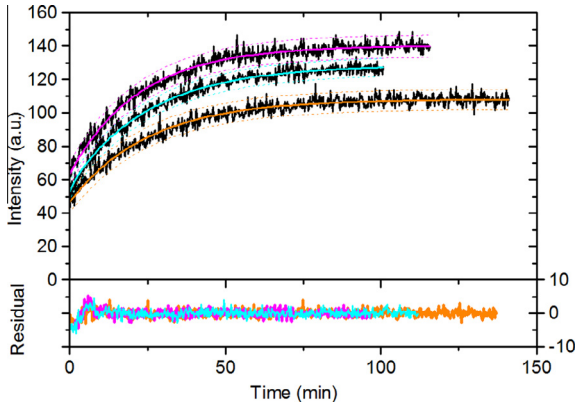


**Fig.4.** Bleaching-corrected emission intensity time profiles during immobilization of epicocconone–MML conjugate in the MPS particles and fitting to a single exponential growth model. Upper panel: Emission traces recorded at particle concentrations of 0.043 g/L (magenta, top spectrum), 0.036 g/L (cyan, middle spectrum), and 0.026 g/L (orange, bottom spectrum). Solid lines are fits to Eq. (1), with the 95% confidence interval for the fits shown as dotted lines Lower panel: Corresponding residuals obtained by subtracting the fits from the experimental data. Data in Fig. 3 were corrected for bleaching as described in Materials and Methods. Protein concentration: $4.5 \times 10^{-8}$ M. (For interpretation of the references to colour in this figure legend, the reader is referred to the web version of this article.)

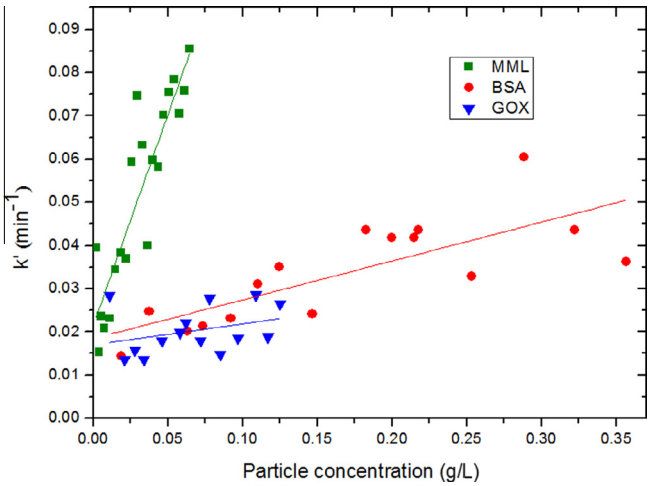


**Fig.5.** Pseudo-first-order rate constants $k'$ versus MPS particle concentration for GOX (blue inverted triangles), BSA (red circles), and MML (green squares). Solid lines are least square linear fits. Second-order rate constants $k$ for each protein were obtained from the slopes using Eq. (S-3b) in the Supplementary material. Protein concentration: $4.5 \times 10^{-8}$ M. (For interpretation of the references to colour in this figure legend, the reader is referred to the web version of this article.)

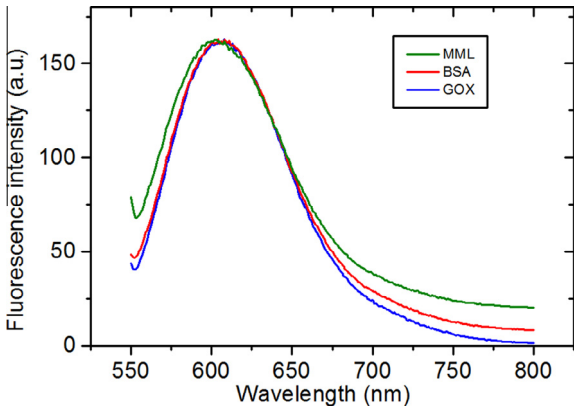


**Fig.6.** Fluorescence emission spectrum of epicocconone bound to MML (green, top spectrum), BSA (red, middle spectrum), and GOX (blue, bottom spectrum) before immobilization of the proteins normalized at the wavelength of maximum intensity (603 nm for MML, 605 nm for BSA and GOX). Excitation wavelength: 520 nm. (For interpretation of the references to colour in this figure legend, the reader is referred to the web version of this article.)

slightly blue shifted with a maximum at 603 nm, but the spectrum is similar enough to the GOX and BSA cases that the fluorescence of epicocconone is deemed to report on the particle interaction in a manner that allows the three proteins to be compared.

### *Bleaching mechanism*

Fig. 7 compares the emission spectra of four identical epicocconone–GOX samples (curve a) with spectra recorded after these samples were incubated for 180 min either under the light conditions used in the collection of the kinetic data (curves c and e) or in the dark (curves b and d). Comparing spectra c and e shows that there is a decrease in the intensity of the illuminated samples and more so in the absence of particles (spectrum e), in agreement with the intensity time profiles for the samples and reference in Fig. 3. However, spectrum b shows that there is a decrease in intensity also when the particle incubation is performed in the dark, albeit to a smaller extent than under illumination (spectrum c). The

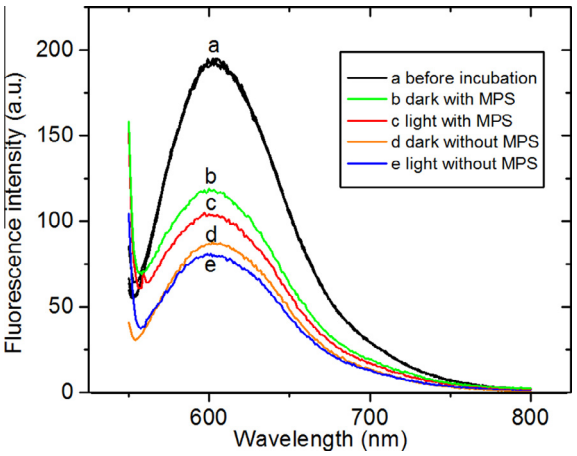


**Fig.7.** Fluorescence emission spectra of epicocconone–GOX conjugate before (curve a) and after incubation for 180 min, either in the dark with the MPS particles present (curve b) or absent (curve d) or under the same illumination conditions as in Fig. 3 with the MPS particles present (curve c) or absent (curve e). Excitation wavelength: 520 nm.

presence of a dark reaction that bleaches the dye is supported by comparing the particle-free incubation experiments in Fig. 6 (curves d and e). The intensity of free epicocconone–protein conjugate decreases also in the dark (curve d) but to a smaller extent than under illumination (curve e).

The results in Fig. 7 indicate that the slow decrease in the emission intensity seen in the particle-free reference in Fig. 3 (black) is due to a combination of a light-dependent process and a dark reaction, both of which bleach the dye. This interpretation was checked by subjecting two identical samples of the free epicocconone–GOX conjugate (no particles) either to continuous illumination as during kinetic data collection (Fig. 3) or to intermittent illumination to reduce the degree of light exposure (5 min off/1 min on). The results in Fig. 8 show that intermittent illumination indeed reduces the rate of intensity decay, which is consistent with the fact that epicocconone is subject to photobleaching. However, it is expected that the dye bleaching should be reduced by approximately 80%

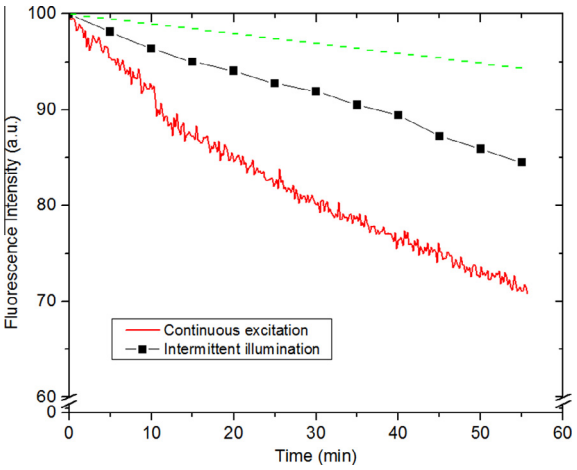


**Fig.8.** Effect of intermittent illumination on epicocconone emission intensity. Two samples of epicocconone–GOX conjugate (without particles) were exposed to continuous excitation (red, bottom line) and to intermittent illumination with light alternatingly off for 5 min and on for 1 min (black, middle line connecting squares that indicate the time intervals of illumination). The dashed line (green, top) corresponds to expected intensity decrease if bleaching is purely photoinduced (5/6 reduction of bleaching). (For interpretation of the references to colour in this figure legend, the reader is referred to the web version of this article.)

(the fraction 5/6 that the light is off); see the upper dashed line in Fig. 8. By contrast, the results in Fig. 7 show that the bleaching of the dye is reduced by only approximately 50%. These observations confirm the existence of two parallel bleaching mechanisms where one does not require light, in contrast to a report [24] that bleaching of epicocconone–protein conjugates is only photoinduced.

## Discussion

### *Mechanism of enhanced emission intensity on particle addition*

Fig. 4 shows that the fluorescence emission intensity of the epicocconone–protein conjugates increases when the MPS particles are added. The presence of the particles may alter the dye fluorescence in at least two ways. The light scattering by the MPS particles may perturb the spectroscopic measurements, or there may be a particle effect on the quantum yield of the dye–protein conjugate when they experience a different microenvironment in the particle pores compared with the surrounding bulk solution.

The MPS particles scatter light according to Rayleigh [25] or Mie [26] theory depending on particle size. First, in both cases, scattering effects are expected to appear on the time scale of seconds needed to mix the added MPS particles in the stirred protein sample, so they cannot explain the slow rise over tens of minutes or longer in Fig. 4. Second, in contrast to the intensity increase we observe when the particles are added, both types of scattering are expected to reduce the detected emission for two reasons. The number of excitation events is reduced by the lower photon flux of excitation light reaching the dye, and furthermore the emitted light may also be scattered and not reach the detector. A related and potentially slow mechanism is a protein-induced aggregation of the particles, but it is also an unlikely explanation because an enhanced scattering by such particle aggregates is again expected to reduce the fluorescence intensity, not to increase it. Third, binding of the epicocconone–protein conjugates to the micron-sized particles arguably leads to a nonrandom distribution of the chromophores in the spectroscopic sample compared with the homogeneous epicocconone–protein solutions before the particles are added. Such inhomogeneity on the length scale of the wavelength of light may have spectroscopic consequences due to altered absorption statistics, but again the expected effect on the measured fluorescence is a lower degree of excitation (and hence emission) due to absorption flattening [27,28] and, thus, cannot explain an increase in intensity.

A more likely explanation for the enhanced emission is that it reflects a change in the fluorescence quantum yield of the dye when the labeled proteins interact with the added particles. Importantly, a different microenvironment inside the MPS particles will have an effect on the dye fluorescence only once the epicocconone is brought inside the pores by the proteins (or possibly in contact with the external particle surface). The time required for such epicocconone–protein–particle interactions to occur can explain why the rise in intensity is slow (see Fig. 3) compared with the essentially instantaneous effects expected from light scattering. It is also worth noticing that the emission increase cannot be explained by the particles partially protecting the immobilized dye–protein from bleaching because then the intensity should still decrease, albeit more slowly. In summary, the increase in intensity with time in Fig. 4 most likely reflects an increased quantum yield due to the dye-labeled proteins interacting with the added MPS particles.

Fluorescent dyes generally are sensitive to properties of the local solvent environment such as polarity, pH, and microviscosity [29], all of which are reflected in changes in emission intensity, spectral shape, or both. In our case, the increase in emission with time at 605 nm in Fig. 4 is due only to a change in intensity and not to a shift of the emission spectrum (or else the intensity would decrease because the monitoring wavelength is no longer at the emission maximum), which is supported by the retained spectral shapes between curves a and b in Fig. 2. The results of other studies based on epicocconone strongly indicate that a different solvent viscosity inside the pores than outside the particles is the more likely explanation for the intensity decrease rather than a different polarity or pH. Studies of epicocconone interacting with cyclodextrins [30] and surfactant assemblies [31] indicate that an enhanced local viscosity increases the emission intensity with unchanged spectral shape of the dye, just as we observe in the presence of the MPS particles, whereas polarity is reported to have no detectable effect on the fluorescence properties of epicocconone. A different pH inside the pores compared with the surrounding solution is also an unlikely source of the intensity increase because the fluorescent probe SNARF-1 attached to lipase reports that the pH inside the MPS particles is close to the external pH in the range used here [12]. The viscosity of water in the pores of MPS particles has not been studied directly to our knowledge, but both experimental nuclear magnetic resonance (NMR) studies [32] and theoretical simulations [33] show that at least close to the pore wall the water molecules are slowed down by interactions with the silica surface. An enhanced local viscosity compared with the solvent outside the MPS particles, therefore, can be expected when the epicocconone–protein conjugates have entered the narrow pores of the MPS particles.

In summary, we ascribe the increase in emission intensity at 605 nm in Fig. 4 to enhanced microviscosity of the local solvent as the dye–protein conjugates interact with the MPS particles, an effect that makes epicocconone fluorescence a useful tool to monitor the protein immobilization in real time. Notably, in this interpretation the intensity increase itself cannot be used to distinguish between pore entry and adsorption to the outside of the MPS particles because the microviscosity might be higher than in bulk solution also close to the external silica surface. Below we show how the question of pore entry can be addressed by using this new fluorescence tool for kinetic studies to investigate the effect of protein size.

### *Comparison with model for protein–particle interaction*

The experimental results in terms of the time profiles in Fig. 4 and the effect of particle concentration on the pseudo-first-order rate constants ($k'$) in Fig. 5 can be compared with a simple model where the protein–particle complex, *EP*, is formed through the reaction

$$E + P \rightarrow EP, \tag{2}$$

where *E* represents free protein and *P* free binding site in the pores of the particle or on its external surface. This model treats all of these binding sites as equivalent, which is clearly a kinetic oversimplification because they might not be equally accessible depending on their location at different depths of the pores, but the model serves to extract some basic understanding on the protein binding to the particles from the data in Fig. 5.

The model in Eq. (2) corresponds to a second-order-rate equation with bimolecular rate constant $k$:

$$d[EP]/dt = k[E][P]. \tag{3}$$

If there is an excess of particles (binding sites) compared with proteins, Eq. (3) has the solution

$$[EP] = [E]_o(1 - e^{-k't}), \tag{4a}$$

where $[E]_o$ is the initial concentration of protein and the pseudo-first-order rate constant $k'$ is predicted to follow

$$k' = k[P]_o, \tag{4b}$$

where $[P]_o$ is the initial particle concentration (see Eq. S-3 in Supplementary material). In terms of the predicted time dependence of the emission intensity, Eq. (4a) is equivalent to Eq. (1) used in the fitting in Fig. 4 (see Eq. S-4).

There are two notable differences between the experimental data (Figs. 4 and 5) and the predictions in Eqs. (4a) and (4b). The small positive deviation early in the residuals of the fits in Fig. 4 indicates that there is a comparatively fast (minutes) binding step, in addition to the predicted single exponential growth in Eq. (4a), that describes the data well for long times. Second, the results in Fig. 5 are in fair accordance with the linear prediction of Eq. (4b), but the fits do not pass through the origin, which suggests that the rate-limiting step in the association process is different at low particle concentrations. These two deviations are probably due to the assumption $[P]_o \gg [E]_o$ that underlies Eq. (4), a condition that seemingly is not fully met under our current conditions given that the final degree of immobilization is approximately 72 to 80% rather than 100% (see Fig. 2). In particular, the condition will be invalid at the lowest particle concentrations, so here we focus on analyzing the second-order rate constant $k$ obtained from the linear fits that describe the kinetic data in the range of high particle concentrations in Fig. 5 and how it is affected by the properties of the proteins.

The main difference among the three proteins studied here is most likely their size. The isoelectric points exhibit a less marked difference, and there is no obvious correlation between the values of $k$ and the p$I$ values (see Table 1). In fact, all three proteins have a negative net charge at the pH 6.0 used in the immobilization experiments, so the binding to the negatively charged silica surface of the MPS particles probably is driven by interactions other than electrostatic. Such a multitude of weaker hydrogen bonding and dispersion forces [5] can be expected to average out and be less protein specific, which leads us to assume that size rather than binding affinity is the most important difference among the three proteins. It may be noted that BSA has a higher degree of dye labeling than the other two proteins (Table 1), and because the neutral epicocconone binds to amine groups on lysine residues [22] that are positively charged at our pH, the less negative BSA (higher p$I$) will in fact approach the net charge of the other two proteins, making them even more comparable.

All three proteins have an approximate globular shape and are modeled as spheres with an effective radius equal to the hydrodynamic radius ($R_H$). Fig. 9 shows how the rate constant $k$ depends on the ratio $R_H/R_{pore}$, where $R_{pore}$ is the average pore radius of the MPS particles (4.6 nm). It is seen that an increased protein size has a strong retarding effect on the immobilization, with an approximately 25-fold lower rate for GOX compared with MML. The higher number of epicocconone dyes attached to BSA may lead to a small increase in its effective size, but if anything such an effect will move the corresponding data point in Fig. 9 that is based on the native size of BSA closer to the fitted curve.

The data in Fig. 9 are well described by a scaling law $k \sim R_H^{-4.7}$ (see curve in Fig. 9), which represents a significantly stronger dependence on protein size than the predicted scaling $k_d \sim R_H^{-1}$ for the bimolecular rate constant ($k_d$) if the reaction between protein and particles is under diffusion control (see Eq. S-6). The much stronger scaling observed experimentally indicates that the immobilization at high particle concentrations is not rate controlled by diffusional encounter between protein and particles but rather is controlled by a process where the rate is more sensitive to protein size. One possible rate-limiting step is then entry of the protein into the pores of the particles (or their diffusion inside the pores), which can be expected to be strongly retarded when the protein radius approaches the average pore radius as in the case of

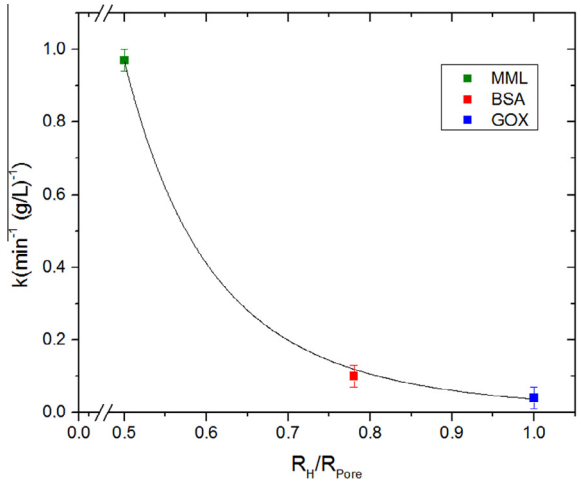


**Fig. 9.** Plot of the second-order rate constant $k$ versus the ratio between the hydrodynamic radii of the proteins ($R_H$) and the pore radius of the MPS particles ($R_{pore}$). The values of $k$ are from the fitted slopes in Fig. 5; error bars are from the quality of the fits. The curve shows the best power law fit $k = aR_H^{-4.70\pm0.01}$ with $a = 42.1$ min$^{-1}$ (g/L)$^{-1}$.

GOX ($R_H$ = 4.5 nm vs. $R_{pore}$ = 4.6 nm). The effective protein radius $R_{eff}$ for pore entry (or intrapore diffusion) is probably smaller than $R_H$ if the transport is limited by steric interactions with the pore walls, but the strong scaling seen in Fig. 9 will remain relevant as long as $R_{eff}$ is proportional to $R_H$.

### *Comparison with other methods to monitor immobilization kinetics*

In a previous study [6], lipase was immobilized in MPS particles of the same SBA-15 type used here and with slightly smaller pores (8.9 nm in diameter). The kinetics was monitored indirectly by using absorbance spectroscopy to measure the amount of protein that remained in the surrounding solution (supernatant) at different times. A detailed comparison with the current work is not possible because approximately 75% of the encapsulation occurred before the first data point (~1 h) and the number of time points were too few to establish a mathematical description of the association kinetics. However, a qualitative agreement can be noted because the MPS particle concentration of 0.04 g/L used by Gustafsson and coworkers [6] is in the lower end of the range covered here (see Fig. 4) and led to immobilization rates similar to ours. The comparison also serves to illustrate the advantage of a direct method that can be used to monitor the immobilization in real time.

Thörn and coworkers [8] used QCM-D to monitor in real time the encapsulation of lipase into mesoporous particles that themselves were adsorbed to a macroscopic surface. The association occurred on a similar time scale as here (a few hours), but again a quantitative comparison cannot be made because the MPS particles were of a different pore type (nonhexagonal) than in the current work. Moreover, in their case the mode of protein transport to the surface-adsorbed particles is likely to be different from that in the suspension of MPS particles used here.

## Conclusions

The main limitation in the current approach is how to correct for the bleaching, which we suspect is the main source of the scattering in the fitted rate constants ($k'$) in Fig. 5. The photobleaching in particular may be slower inside the particles than in the particle-free reference sample due to absorption

flattening, and the nature of the dark reaction needs to be better understood to improve the correction for the bleaching. Using a dye that is less prone to bleaching (at least in the dark) may be another approach to overcome this problem. The bleaching will have a direct effect on the measurements of the degree of immobilization, which therefore are only estimates, but it is only a second-order effect in the kinetic measurements and will not affect our main conclusion that at high particle concentrations the rate-limiting step most likely is the protein entry into the pores.

The lack of agreement between the simple model and the results at low particle concentrations suggests that other factors, such as protein transport outside the pores, may influence the binding kinetics under these conditions. The deviation in the fits of the intensity time profiles for the first few minutes (Fig. 4) also need to be studied in more detail to investigate the role of binding to the external particle surface as a potential intermediate state in the immobilization process. The time resolution in the current manual mixing protocol is not good enough for processes that occur on the time scale of minutes or faster and probably need to be studied by fluorescence-detected stopped-flow methods.

## Acknowledgments

Hanna Gustafsson is thanked for MPS particle synthesis and characterization. A Linnaeus grant SUPRA to B.Å. from the Swedish Research Council is thankfully acknowledged.

## Appendix A. Supplementary data

Supplementary data associated with this article can be found, in the online version, at http://dx.doi.org/10.1016/j.ab.2015.02.005.

## References

[1] J.M. Rosenholm, V. Mamaeva, C. Sahlgren, M. Linden, Nanoparticles in targeted cancer therapy: mesoporous silica nanoparticles entering preclinical development stage, Nanomedicine 7 (2012) 111–120.
[2] I.I. Slowing, J.L. Vivero-Escoto, C.W. Wu, V.S. Lin, Mesoporous silica nanoparticles as controlled release drug delivery and gene transfection carriers, Adv. Drug Deliv. Rev. 60 (2008) 1278–1288.
[3] S. Hudson, J. Cooney, E. Magner, Proteins in mesoporous silicates, Angew. Chem. Int. Ed. 47 (2008) 8582–8594.
[4] C.H. Lee, T.S. Lin, C.Y. Mou, Mesoporous materials for encapsulating enzymes, Nano Today 4 (2009) 165–179.
[5] N. Carlsson, H. Gustafsson, C. Thörn, L. Olsson, K. Holmberg, B. Åkerman, Enzymes immobilized in mesoporous silica: a physical–chemical perspective, Adv. Colloid Interface Sci. 205 (2014) 339–360.
[6] H. Gustafsson, C. Thörn, K. Holmberg, A comparison of lipase and trypsin encapsulated in mesoporous materials with varying pore sizes and pH conditions, Colloids Surf. B 87 (2011) 464–471.
[7] M.M. Bradford, A rapid and sensitive method for the quantitation of microgram quantities of protein utilizing the principle of protein–dye binding, Anal. Biochem. 72 (1976) 248–254.
[8] C. Thörn, H. Gustafsson, L. Olsson, QCM-D as a method for monitoring enzyme immobilization in mesoporous silica particles, Microporous Mesoporous Mater. 176 (2013) 71–77.
[9] L. Whitmore, B.A. Wallace, Protein secondary structure analyses from circular dichroism spectroscopy: methods and reference databases, Biopolymers 89 (2008) 392–400.
[10] R.Y. Tsien, The green fluorescent protein, Annu. Rev. Biochem. 67 (1998) 509–544.
[11] M. Chalfie, Green fluorescent protein, Photochem. Photobiol. 62 (1995) 651–656.
[12] C. Thörn, N. Carlsson, H. Gustafsson, K. Holmberg, B. Åkerman, L. Olsson, A method to measure pH inside mesoporous particles using protein-bound SNARF1 fluorescent probe, Microporous Mesoporous Mater. 165 (2013) 240–246.
[13] A. Yamaguchi, M. Namekawa, T. Kamijo, T. Itoh, N. Teramae, Acid–base equilibria inside amine-functionalized mesoporous silica, Anal. Chem. 83 (2011) 2939–2946.
[14] S.-I. Matsuura, T. Itoh, R. Ishii, T. Tsunoda, K. Sakaguchi, T. Hanaoka, F. Mizukami, Encapsulation of fluorescent proteins in folded-sheet mesoporous materials: effect of pore size on energy-transfer efficiency, Microporous Mesoporous Mater. 131 (2010) 245–251.
[15] S. Hudson, E. Magner, J. Cooney, B.K. Hodnett, Methodology for the immobilization of enzymes onto mesoporous materials, J. Phys. Chem. B 109 (2005) 19496–19506.
[16] H. Gustafsson, E.M. Johansson, A. Barrabino, M. Odén, K. Holmberg, Immobilization of lipase from *Mucor miehei* and *Rhizopus oryzae* into mesoporous silica: the effect of varied particle size and morphology, Colloids Surf. B 100 (2012) 22–30.
[17] C. Thörn, H. Gustafsson, L. Olsson, Immobilization of feruloyl esterases in mesoporous materials leads to improved transesterification yield, J. Mol. Catal. B 72 (2011) 57–64.
[18] D.Y. Zhao, Q.S. Huo, J.L. Feng, B.F. Chmelka, G.D. Stucky, Nonionic triblock and star diblock copolymer and oligomeric surfactant syntheses of highly ordered, hydrothermally stable, mesoporous silica structures, J. Am. Chem. Soc. 120 (1998) 6024–6036.
[19] K. Hirayama, S. Akashi, M. Furuya, K. Fukuhara, Rapid confirmation and revision of the primary structure of bovine serum albumin by ESIMS and Frit–FAB LC/MS, Biochem. Biophys. Res. Commun. 173 (1990) 639–646.
[20] C.H. Lei, T.A. Soares, Y.S. Shin, J. Liu, E.J. Ackerman, Enzyme specific activity in functionalized nanoporous supports, Nanotechnology 19 (2008), http://dx.doi.org/10.1088/0957-4484/19/12/125102.
[21] G. Zoldak, A. Zubrik, A. Musatov, M. Stupak, E. Sedlak, Irreversible thermal denaturation of glucose oxidase from *Aspergillus niger* is the transition to the denatured state with residual structure, J. Biol. Chem. 279 (2004) 47601–47609.
[22] D.R. Coghlan, J.A. Mackintosh, P. Karuso, Mechanism of reversible fluorescent staining of protein with epicocconone, Org. Lett. 7 (2005) 2401–2404.
[23] J.A. Mackintosh, D.A. Veal, P. Karuso, FluoroProfile, a fluorescence-based assay for rapid and sensitive quantitation of proteins in solution, Proteomics 5 (2005) 4673–4677.
[24] G.B. Smejkal, M.H. Robinson, A. Lazarev, Comparison of fluorescent stains: relative photostability and differential staining of proteins in two-dimensional gels, Electrophoresis 25 (2004) 2511–2519.
[25] J. Strutt, On the scattering of light by small particles, Philos. Mag. Series 4 (41) (1871) 447–454.
[26] G. Mie, Beiträge zur Optik trüber Medien, speziell kolloidaler Metallösungen, Annalen der Physik 330 (1908) 377–445.
[27] C. Bustamante, M.F. Maestre, Statistical effects in the absorption and optical activity of particulate suspensions, Proc. Natl. Acad. Sci. USA 85 (1988) 8482–8486.
[28] P.J. Halling, Estimation of flattening coefficient for absorption and circular dichroism using simulation, Anal. Biochem. 387 (2009) 76–81.
[29] J.R. Lakowicz, Principles of Fluorescence Spectroscopy, third ed., Springer, New York, 2011.
[30] T.N. Burai, D. Panda, A. Datta, Fluorescence enhancement of epicocconone in its complexes with cyclodextrins, Chem. Phys. Lett. 455 (2008) 42–46.
[31] D. Panda, S. Khatua, A. Datta, Enhanced fluorescence of epicocconone in surfactant assemblies as a consequence of depth-dependent microviscosity, J. Phys. Chem. B 111 (2007) 1648–1656.
[32] B. Grünberg, T. Emmler, E. Gedat, I. Shenderovich, G.H. Findenegg, H.H. Limbach, G. Buntkowsky, Hydrogen bonding of water confined in mesoporous silica MCM-41 and SBA-15 studied by 1H solid-state NMR, Chemistry 10 (2004) 5689–5696.
[33] K. Shirono, H. Daiguji, Molecular simulation of the phase behavior of water confined in silica nanopores, J. Phys. Chem. C 111 (2007) 7938–7946.

# A fluorescence spectroscopy assay for real time monitoring of enzyme immobilization into mesoporous silica particles.

Pegah S. Nabavi Zadeh[a], Kassam Abdel Mallak[a], Nils Carlsson[a,b], Björn Åkerman[a,*]

[a] Chalmers University of Technology, Department of Chemical and Biological Engineering, Physical Chemistry, SE-41296 Gothenburg, Sweden
[b] Present adress Borealis AB, SE-444 86 Stenungsund, Sweden

[*]Corresponding author
[*]baa@chalmers.se

## Supporting material.

### 1. Effect of MPS particles on the emission spectra of epicocconone/protein conjugates

Figure S-1 shows the changes in the emission spectrum during MPS-incubation with the epicocconone conjugates of GOX and BSA, the degree of immobilization is comparably high at 83% for GOX and 75% for BSA.

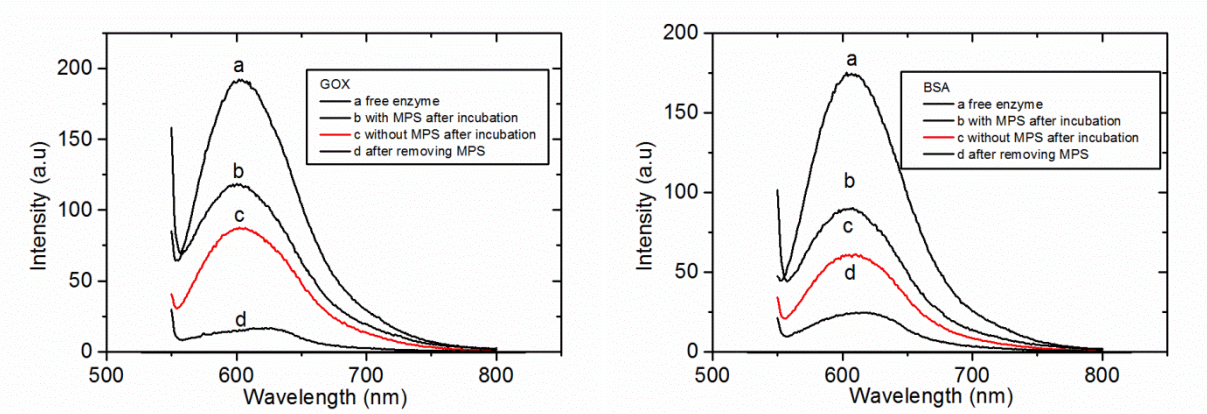


Figure S-1. Emission spectra of epicocconone conjugates with GOX (left) and BSA (right). (a) free enzyme before the particles have been added, (b) after illuminated incubation with MPS for 180 minutes, (c) after illumination for 180 minutes without MPS, and (d) the supernatant after the particles in the sample of curve (b) have been removed by centrifugation. Excitation wavelength 520 nm. Particle concentration 0.055 g/l, protein concentration $4.5\times10^{-8}$ M.

### 2. Experimental fluorescence time-profile with GOX at high particle concentration.

Figure S-2 shows that a significant spike appears in the fluorescence intensity with GOX on the time scale of minutes upon particle addition at MPS concentrations higher than 0.14 g/l.

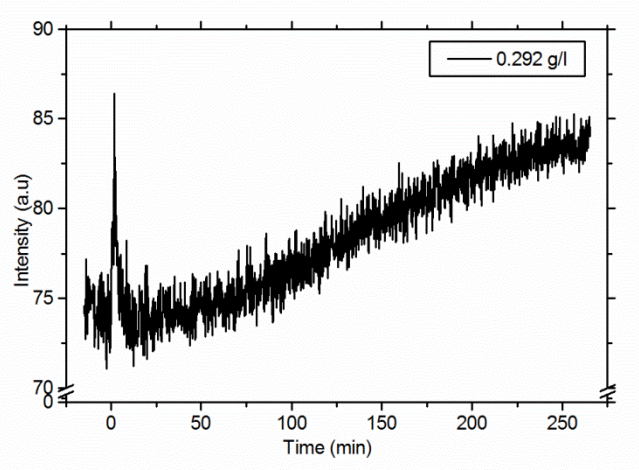


Figure S-2. Emission intensity time profile during immobilization of epicocconone/GOX conjugate at a MPS concentration of 0.292 g/l.

## 3. Theory for fluorescence time-response during the enzyme-particle association.

Assuming that the formation of the protein/particle complex *EP* is a second order reaction with rate constant *k* gives

$$d[EP]/dt = k[E][P] \qquad \text{(S-1)}$$

where *E* and *P* represents free protein and free binding sites in the particles. The general solution for the concentration *[EP]* of immobilized protein at time t is given by[1]

$$kt = 1/([P]_o-[E]_o)\cdot ln\{[E]_o([P]_o-[EP])/[P]_o([E]_o-[EP])\} \qquad \text{(S-2)}$$

where $[P]_o$ and $[E]_o$ are the initial concentrations of particles and protein, respectively ($[P]_o \neq [E]_o$). If it is assumed that the particles provide an excess of binding sites for the proteins ($[P]_o >> [E]_o$) the general solution in (S2) can be simplified to

$$[EP](t) = [E]_o(1-exp(-k't)) \qquad \text{(S-3a)}$$

where

$$k' = k([P]_o-[E]_o) \approx k[P]_o \qquad \text{(S-3b)}$$

Equations (S-3) correspond to equations (5) of the main text. Equation (S-3b) predicts that $k'$ is proportional to the initial particle concentration with slope *k*, the second order rate constant.

If the interaction (immobilization) of the dye/protein conjugate with the particles alters the apparent quantum yield $q$ of fluorescence at the used wavelength by a factor of $\beta$, the time dependence of the resulting emission intensity $I$ is given by (using $[E] = [E]_o - [EP]$)

$$I(t) = q[E] + \beta q[EP] = q[E]_o + (\beta-1)q[E]_o(1-\exp(-k't)) \qquad \text{(S-4)}$$

which is equation (2) of main text with $I_o = q[E]_o$ and $A = q(\beta-1)[E]_o$.

The bimolecular rate constant $k_d$ for diffusion controlled binding of proteins to particles can estimated as follows. For two spheres in free solution[1]

$$k_d = 4\pi N_A(R_{part} + R_{prot})(D_{part} + D_{prot}) \qquad \text{(S-5)}$$

where $D_{prot}$ and $D_{part}$ are the diffusion coefficients for the protein and particles respectively, and $R_{prot}$ and $R_{part}$ the corresponding radii. The particle radius (average value 500 nm for the MPS used here) is much larger than the protein radius ($R_H$ <5nm for the proteins in this study). Consequently the diffusion coefficient $D_{prot}$ can be assumed to be much larger than the diffusion coefficient of the $D_{part}$, using the diffusion coefficient $D = k_BT/6\pi\eta R$ of a sphere with radius $R$ where $\eta$ is the solvent viscosity, $k_B$ is the Boltzmann constant and $T$ is the absolute temperature. Equation (S-5) then gives

$$k_d = 2R_{part}k_BTN_A/3\eta R_H \qquad \text{(S-6)}$$

which predicts that $k_d$ scales as $R_H^{-1}$.

## References

1. Atkins P, Paula J, Friedman R. *Quanta, matter and change. A molecular approach to physical chemistry*. Oxford University Press, Oxford, England, 2009.

***Paper II***

# Rotational mobility and pore filling of enzymes confined in mesoporous silica particles studied by steady state fluorescence anisotropy

Pegah S. Nabavi Zadeh, Björn Åkerman*

Chalmers University of Technology, Department of Chemistry and Chemical Engineering, Physical Chemistry, SE-41296 Gothenburg, Sweden

*corresponding author
*baa@chalmers.se

## Abstract

Enzyme immobilization in mesoporous silica particles is used to improve the enzyme function in biocatalytic application. Here, we used steady state fluorescence anisotropy as a technique to investigate if immobilized proteins can rotate inside the pores more slowly than the same proteins in free solution or if the immobilized proteins are adsorbed to the pores walls which in this case are expected to rotate with the rotation rate of the particles as a single system. The proteins immobilized in different mesoporous silica particles are lipase and bovine serum albumin which the fluorescence of their intrinsic aromatic amino acids is used for monitoring the rotational mobility of the immobilized and the free-solution proteins. Two different conditions are examined first the effect of relative pore size compared to protein size and second the effect of different mesoporous particle dimeter and shape on rotational mobility and pore filling of the proteins. As the results, we discuss that by decreasing the pore size, both proteins after immobilization rotate more slowly, however, size of the mesoporous particle cannot be an important factor. Pore filling ($P_f$) and number of proteins per particle ($N_{prot}$) calculated in each condition show that $P_f$ values can decrease in smaller pore size and the larger particles can accommodate many more proteins which scales with the linear particle diameter (D) $N_{prot} \sim D^{2.94+/-0.01}$ for MML and $N_{prot} \sim D^{2.95+/-0.01}$ for BSA which means both proteins are well-distributed in the particles. At the end three different possible mechanisms that retard the rotational mobility and pore filling are discussed.

**Key words:** Immobilized enzymes, Mesoporous silica, Fluorescence anisotropy, Rotational mobility, Pore filling

## 1. Introduction

Enzyme immobilization for biocatalytic applications is commonly used to improve enzyme stability and function, as well as for easy recovery of both product and enzyme (1, 2). Mesoporous silica (MPS) particle is a common support material for enzyme immobilization due to advantageous properties such as a large surface area, a narrow pore size distribution, and high chemical and thermal stability of the particle material. The porous structure allows for high enzyme loadings and creates a protective environment where the enzymes sometimes can tolerate elevated temperature and high salt concentration (3). Several spectroscopic studies have been performed in order to better understand the mechanism behind of the enzyme immobilization process which is not yet fully understood (4-6). A common indirect method for studying immobilization is to perform spectroscopic measurements on the solution surrounding the particles in the form of the supernatant after the particles have been removed by centrifugation (3, 7). However, some recent studies have introduced spectroscopic methods that allow for the direct monitoring of the immobilization process. For example, fluorescence spectroscopy has been used to measure the pH sensed by immobilized proteins inside the pores of the silica particles, using enzymes which were modified covalently with the fluorescent pH-probe SNARF1 (8) or the pore walls with the dye pyranine (9). More recently we have shown how a fluorescence spectroscopy assay with dye-labelled proteins can be used to monitor the whole immobilization process in real time (5). Less is understood regarding the dynamic behaviour of proteins inside the pores of the particles. This aspect of enzyme immobilization is of interest for understanding the physical properties of these macromolecules under confining conditions, including the possible significance of structural fluctuations in the proteins for the catalysis and enzyme activity of biocatalyst in general (10, 11). Fluorescence anisotropy is an established spectroscopic technique to investigate the dynamic properties of proteins, making this method is a powerful tool in biochemical research and medical analysis (12, 13). Two

examples are the rotational mobility of fluorescent ligands that bind to proteins (14), and measurements of the hydrodynamic molecular size of (dye-labeled) proteins in bulk solution including organic solvents (15). However, to our knowledge fluorescence anisotropy has not been applied in studies of the dynamic behavior of enzymes immobilized in porous particles. Here we investigate whether fluorescence anisotropy can be used to monitor the rotational mobility of enzymes inside the particle pores.

Rotation of immobilized proteins may seem like a contradiction in terms, but by immobilization we mean here that the leakage into the external solution is prevented, a desirable effect in applications sometimes referred to as encapsulation. Such restrictions on the translational motion does not necessarily mean that the proteins cannot rotate to a certain degree inside the pores, depending on the mechanism and strength of the forces responsible for the immobilization. An illustrative example is when a water soluble proteins such as lipase are immobilized in water filled pores of mesoporous silica particles suspended in an organic solvent containing the (lipophilic) substrate of the lipase. The protein is immobilized mainly by its low solubility in the external phase, by confining forces which do not necessarily restrict its rotation inside the pores. In fact, the possibility to rotate may be crucial so that the active site can face the substrate in the external solution.

Our main aim was to develop a technique that allows for investigating if a protein can undergo rotation inside the pores, albeit possibly more slowly than in free solution, or if the protein is adsorbed to the pore walls in which case the immobilized enzymes are expected to rotate with a rate governed by the rotation of the particles as a whole. To this end we use steady state fluorescence anisotropy of intrinsic aromatic amino acids to monitor the rotational motion of two different enzymes (lipase and bovine serum albumin) which are immobilized in MPS particles, and compare with the rotational rate of the same enzymes when free in an aqueous solution. We investigate the influence of relative pore size compared to protein size by

immobilizing the two enzymes into mesoporous silica particles with two different pore radii but the same particle size and shape. Secondly the two proteins were immobilized into four types of mesoporous silica particles with the same pore size but different particle diameters and morphology in order to investigate the effect of particle size and shape on the mobility of the immobilized enzymes.

As opposed to our previous work (5, 8) no fluorescent labelling was needed since we exploit the anisotropy of the intrinsic aromatic amino acid residues, with the intention to minimize the rotation of the chromophore itself by avoiding dyes linked to the protein by a flexible linker. The proteins studied here contains both tryptophan and tyrosine, but the indole group of tryptophan residues is the dominant source of absorption and emission in proteins in the near UV-region. Both tryptophan and tyrosine residues can be excited at 280 nm but the emission maximum of tryptophan is at 350nm while tyrosine emission is at 300nm and more narrowly distributed (16). Thus, under our spectroscopic conditions (excitation at 280nm, emission at 350nm) the main contributing chromophore is tryptophan. A challenge is then the comparatively high turbidity of particle-containing samples at 280 nm compared to the longer excitation wavelengths available with extrinsic fluorescent protein labels which often are designed to absorb in the visible region.

## 2. Materials and methods

### 2.1. Chemicals and particles

Lipase (MML from *Mucor Miehei*) and albumin (BSA from *bovine serum*) were purchased from Sigma-Aldrich. The properties of the proteins in this study can be found in table1. No dye labeling was performed because the tryptophan residues in both MML and BSA were used as intrinsic fluorescent reporters. If not otherwise stated, the experiments were performed in 0.1M phosphate citrate buffer (disodium phosphate and trisodium citrate) at pH = 6 and 25$^{\circ}$C

**Table1. Properties of the proteins**

| Protein[a] | $M_w$[b] (kD) | $R_H$[c] (nm) | $pI$[d] | $\varepsilon_{280}$[e] ($M^{-1}cm^{-1}$) | $\tau_{(Trp)}$[f] (ns) | $\theta_{prot\ free}$[g] (ns) |
|---|---|---|---|---|---|---|
| MML | 32 | 2.25 | 3.8 | 42800 | 3.5 | 23.6 |
| BSA | 66 | 3.5 | 4.7 | 43824 | 6.3 | 88.8 |

a. MML-Mucor Miehei Lipase, BSA-Bovine Serum Albumin
b. Molecular weight (17, 18)
c. Hydrodynamic radius (7, 8)
d. Isoelectric point (17, 18)
e. Extinction coefficient (7, 8)
f. Average excited state lifetime of tryptophan residues (19, 20)
g. Global rotation correlation time for free protein estimated by equation (8).

Mesoporous silica (MPS) particles of types SBA-15 and HMM were a gift of Hanna Gustafsson (Applied chemistry, Chalmers) and were synthesized as described previously (7, 21). Nitrogen adsorption was used for characterization the MPS to obtain average pore diameter, specific pore volume and BET surface area. Four types of mesoporous silica particle with the same pore radius and different particle diameter were used, as well as two types of particles with the same particle diameter but different pore size. The properties of the used MPS are summarized in table 2.

**Table 2. Properties of the MPS particles**

| MPS-*D*[a] | Type[b] | *BJH* pore size[c] (nm) | *BET* surface area[d] ($m^2/g$) | $V_{pore}$[e] ($cm^3/g$) | $\theta_{part}$[f] (s) |
|---|---|---|---|---|---|
| MPS-40 | HMM | 9.1 | 463 | 0.91 | $8.5 \cdot 10^{-6}$ |
| MPS-300 | SBA-15 | 9.4 | 606 | 1.03 | $3.5 \cdot 10^{-3}$ |
| MPS-1000 | SBA-15 | 9.3 | 502 | 1.18 | $1.2 \cdot 10^{-1}$ |
| MPS-2000 | SBA-15 | 8.9 | 554 | 1.17 | 1.1 |
| MPS-2000 | SBA-15 | 6.0 | 986 | 1.08 | 1.1 |

a. MPS-*D*: Mesoporous silica particles, where *D* refers to the average particle diameter in nm (7, 21)
b. Type of MPS preparation. HMM: Hiroshima Mesoporous Materials, SBA-15: Santa Barbara Amorphous (7, 21)
c. Average pore diameter obtained by the Barret-Joyner-Halenda method (7, 21)
d. Surface area obtained by the Brunauter-Emmett-Teller method (7, 21)
e. Total specific pore volume obtained by the nitrogen adsorption-desorption isotherms (7, 21)
f. Estimated rotational correlation time for particles calculated by equation (6) for a spherical particle, using the average particle radius $R_{part} = D/2$, see section 2.4.

The morphology of the particles were investigated by SEM (See Figure 1). It is seen that the MPS-40 particles (Fig.1a) are essentially spherical, MPS-300 (Fig.1b) and MPS-2000 (Fig.1d) rod-like, whereas the MPS-1000 particles (Fig.1c) are disc-like in shape.

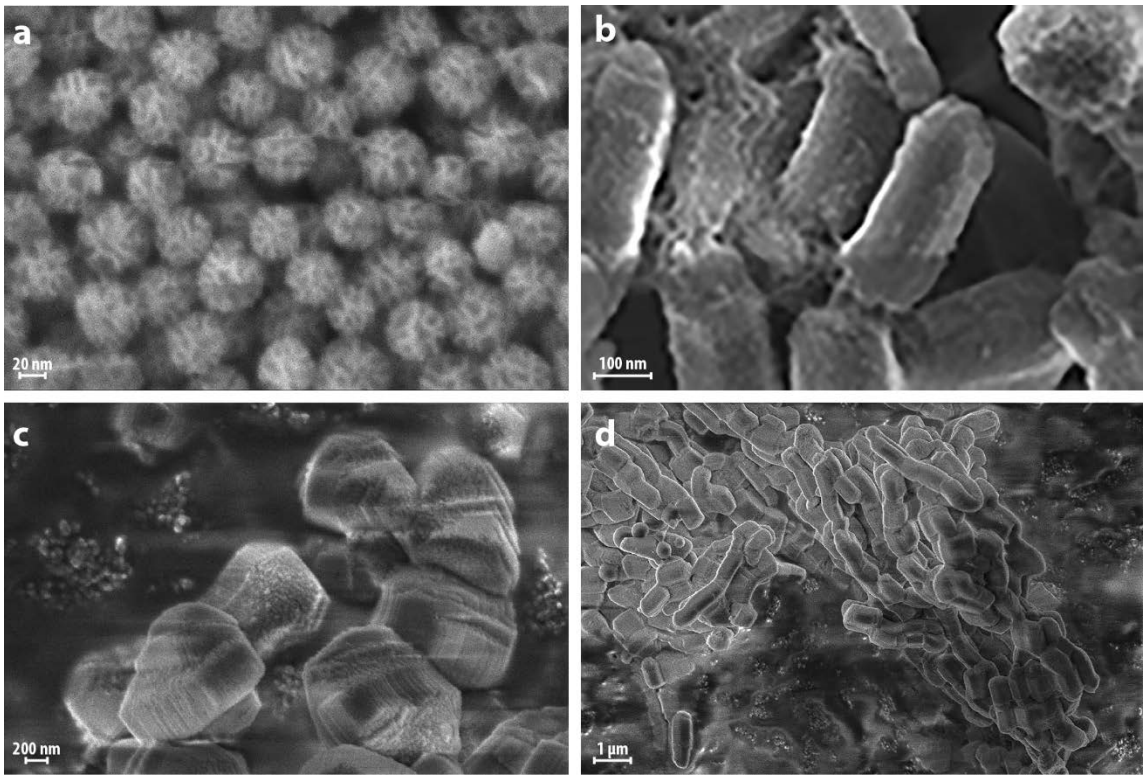


Figure 1. Morphology of the MPS particles by SEM imaging. (a) MPS-40, spherical particles with slit-shaped pores without an ordered structure; (b) MPS-300, rod-shaped with hexagonally ordered uniform pores; (c) MPS-1000, disc-like with hexagonally ordered pores; (d) MPS-2000, rod-shaped with hexagonally ordered pores (7, 21).

## 2.2. Protein immobilization

Aqueous solutions of the MPS were prepared by dispersing 5 mg of dry mesoporous silica particles in 1ml phosphate-citrate buffer, using vortexing for 10 min at 10 rpm followed by sonication (Ultrasonic cleaner model CD-4800 at a power of 70 W) for 20 min in order to dissolve any particle aggregates, and a final step of vortexing for 5min.

Protein-particle samples were prepared by mixing 20µl of MML or BSA stock solution (20mg/ml in phosphate-citrate buffer) with 200 µl of MPS solutions (5mg/ml) diluted to a final volume of 500 µl with phosphate-citrate buffer. Each sample contained a total amount of 400 µg enzyme/mg MPS. The samples were then incubated at 25°C for 48 h during gentle stirring,

and then centrifuged for 6 min. The pelleted protein-particles conjugates were re-suspended, and washed three times with 500 µl of phosphate citrate buffer by repeated centrifugation and resuspension. The purified MPS particles with immobilized proteins were finally re-suspended by adding 100 µl of buffer and vortexing for a few minute until homogenous samples were obtained for the spectroscopic measurements.

The fraction of the added protein which were associated with the particles (degree of immobilization DOI) and the protein loading $P_{LD}$ (µg protein/mg particle) of the two different enzymes in each particle type were calculated from the difference between the total added amount of enzyme and the amount of remaining enzyme in the supernatant after particle washing, measured by UV absorption at 280 nm using a Varian cary50 spectrophotometer.

The amount of immobilized protein was expressed as the number $N_{prot}$ of proteins per particle, calculated as (22)

$$N_{prot} = N_A \cdot P_{LD} \cdot V_{part} \cdot \rho_{part} / M_W \qquad (1a)$$

where $N_A$ is Avogadro's number, $M_w$ the molecular weight of the proteins (Table 1), $V_{part}$ is the average volume per particle assumed to be a sphere with diameter $D$ (Table 2) and $\rho_{part}$ is the density of the dry porous particles calculated from the particle porosity Φ as

$$\rho_{part} = \rho_{silica}(1-\Phi) = \rho_{silica}(1-V_{pore}/(V_{pore} + \rho_{silica}^{-1})) \qquad (1b)$$

where $\rho_{silica}$ = 2.196g/cm$^3$ is the density of amorphous silica (23). The actual protein concentration in the pores was expressed in terms of the pore filling $P_f$ defined as the fraction of the available pore volume which is occupied by proteins, and calculated as

$$P_f = V_{prot}/V_{pore} = \frac{4\pi}{3} R_H^3 N_A (P_{LD}/M_W)/V_{pore} \qquad (1c)$$

where $V_{pore}$ is the total pore volume per gram of the particles (see Table 2), and where the volume $V_{prot}$ of protein per gram of particles is calculated assuming each protein is a sphere with a radius equal to the hydrodynamic radius $R_H$ (Table 1).

## 2.3. Spectroscopic measurements

When a fluorescent molecule is excited with polarized light, the resulting fluorescence emission is also polarized, but to a lesser degree due to depolarizing processes including rotational diffusion of the fluorophore during its excited-state lifetime. Steady state fluorescence anisotropy (r) is an experimental measure of fluorescence depolarization which can be used to monitor the rotational mobility of a fluorophore (16). Anisotropy is measured by exciting the fluorophore with linearly polarized light and measuring the fluorescence intensity both parallel and perpendicular to the excitation polarization direction. Steady state emission anisotropy spectra were recorded on a SPEX fluorolog3 spectrofluorimeter (JY Horiba) using Glan polarizers, excitation was performed at 280 nm and emission recorded in the wavelength range from 300 to 450 nm. Excitation and emission slit width was 6nm.

The fluorescence anisotropy was calculated as (13)

$$r = \frac{I_{VV} - G I_{VH}}{I_{VV} + 2G I_{VH}} \qquad (2)$$

where $I_{XY}$ is the emitted intensity and the subscripts X and Y indicate the polarization directions of the excitation and emission light, respectively, with H and V referring to horizontal and vertical, and where the instrumental correction factor G is given by

$$G = \frac{I_{HV}}{I_{HH}} \qquad (3)$$

Figure 2 shows typical emission spectra recorded for free BSA at the four different combinations of polarizer directions. Each emission component was corrected for light scattering by subtracting a spectrum of a protein-free particle sample with the same setting of

the polarizers. Scattering contributions were minimized by using an excess of added enzyme (400µg enzyme/mg MPS) in order to ensure high protein loading in the particles. The particles were washed three times with protein-free buffer before the spectroscopic measurements in order to remove free and/or loosely bound proteins, and leakage of proteins during the spectroscopic measurements were monitored and corrected for by measuring free enzyme in the supernatant obtained by centrifugation after the spectroscopic measurements.

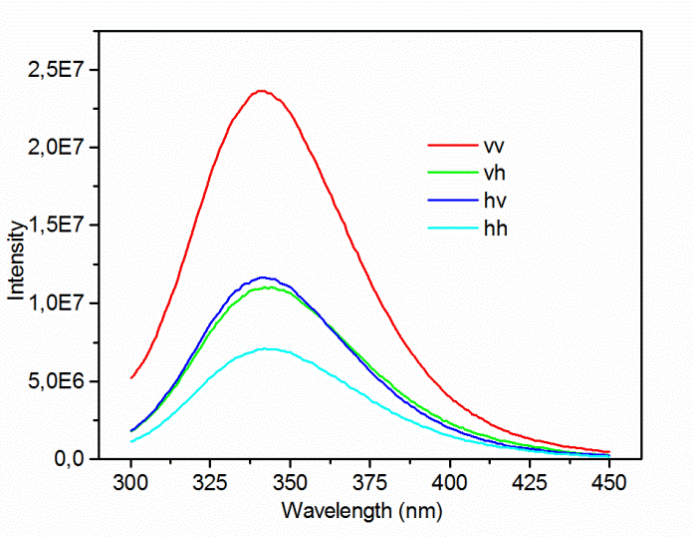


Figure 2. Polarized emission spectra of free BSA with the indicated orientation of the excitation and emission polarizers.

Figure 3 shows typical results (for the sample with free BSA) in terms of the anisotropy spectra ($r$) calculated by equation (2) and the corresponding total intensity ($I_{tot}$) calculated as (16)

$$I_{tot} = I_{vv}+2GI_{vh} \qquad (4)$$

The anisotropy values presented below for each combination of protein and MPS were taken as the average value in the range 335-355nm, with the uncertainty calculated from the variation between 3 and 4 independent experiments.

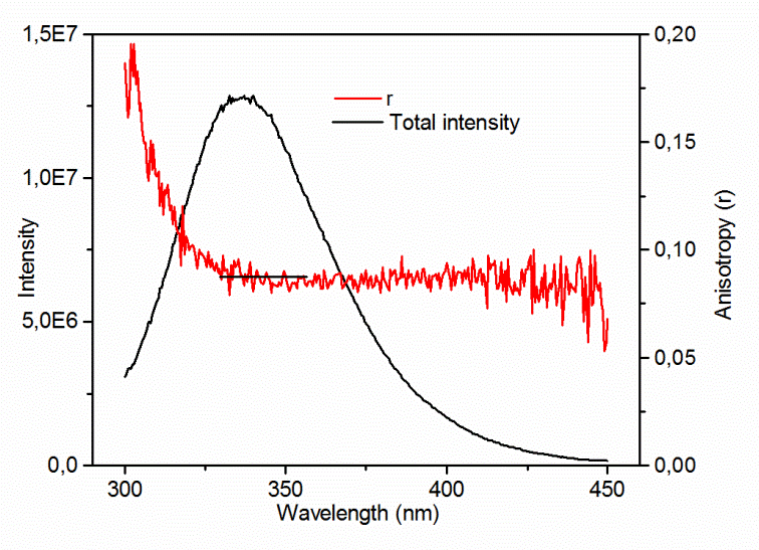


Figure 3. Spectra for anisotropy *r* and total intensity $I_{tot}$ for free BSA calculated from the components in Figure 2 using equations (2) - (4). Solid horizontal black line represents the used average value of the anisotropy.

## 2.4. Theory

The fluorescence anisotropy of a fluorophore is a measure of its rotational mobility on the timescale of the fluorescence lifetime. For a protein with a single fluorophore with lifetime ($\tau$), the rotational correlation time ($\theta$) is related to the steady state anisotropy ($r$) through the Perrin equation (13, 16)

$$r = \frac{r_0}{1+\frac{\tau}{\theta}} \qquad (5)$$

where $r_o$ is the fundamental anisotropy of the fluorophore in the absence of rotational motion, which for the tryptophan chromophore is $r_o = 0.3$ (13, 16). The value of the lifetime is generally sensitive to the environment so $\tau$ differs slightly between the two proteins studied here (see Table 1). In addition both proteins contain four tryptophan residues, so the lifetimes in Table 1 correspond to an average value.

For a spherical particle with radius *R*, the rotation correlation time ($\theta$) in equation (5) is given by

$$\theta = \frac{\eta \frac{4}{3}\pi R^3}{k\,T} \qquad (6)$$

where $\eta$ is the solution viscosity, $k$ is Boltzmann constant and $T$ the temperature. For a dilute protein solution the viscosity can be approximated by that of pure water $\eta_o$= 1.0020 mPa·s at 20°C. For a non-dilute protein solution the rotation is expected to be retarded by interactions with neighboring proteins. On the nanosecond time scale probed by fluorescence anisotropy the retardation is mainly due to hydrodynamic interactions (24), steric effects due to collisions with other proteins only play a role at longer time scales. Banchio and Nägele (25) have investigated how an increased concentration decreases the short-time rotational diffusion coefficient ($D_{rot}$) in a non-dilute solutions of spheres, and by using $\theta = 1/6D_{rot}$ (16) their results can be used to estimate how the rotational correlation time is increased in a non-dilute solution of proteins

$$\theta = \theta_o / (1 - 1.3\phi^2) \qquad (7)$$

where $\phi$ is the volume fraction of proteins and $\theta_o$ is the rotational correlation time in the limit of a dilute solution, obtained from equation (6) with $\eta = \eta_o$.

In the case of a rigidly attached fluorophore, the protein radius $R$ calculated from the anisotropy measured for (non-immobilized) protein using equations (5) and (6) is expected to be close to the hydrodynamic radius ($R_H$) obtained by direct hydrodynamic methods such as dynamic light scattering. It is well established, however, that in the case of tryptophan residues in proteins the fluorophore undergoes a local segmental motion relative to the protein matrix which contributes to the depolarization in addition to overall protein rotation (11, 26). Applying the Perrin equation (5) to the measured anisotropy then gives apparent rotational correlation time $\theta_A$, and the corresponding apparent radius ($R_A$) of the protein obtained from equation (6) may then be smaller than the hydrodynamic radius, because a fraction of the total anisotropy is lost due to the segmental motion of the tryptophan fluorophore itself and the protein appears to rotate faster. The correlation time ($\theta_{prot}$) for the global protein rotation can be estimated (11, 27) by

using the know hydrodynamic radii $R_H$ of the proteins (Table 1) in a modified version of equation (6)

$$\theta_{prot} = f\frac{\eta\frac{4}{3}\pi R_H{}^3}{k\,T} \qquad (8)$$

where $f$ is a factor depending on the shape and hydration of the protein, for globular proteins assuming the value $f$ = 2. For free MML and BSA the so predicted values of $\theta_{prot}$ under our conditions are 23.6 and 88.8 ns, respectively (See Table 1).

In our system of proteins immobilized in porous particles an additional process that potentially affects the anisotropy is rotation of the whole MPS particle, occurring with a rotational correlation time we denote $\theta_{part}$. For example, in the case of a protein which is strongly adsorbed to the pore wall the rate of rotation will be zero relative to a coordinate system fixed to the particle ($\theta_{prot} = \infty$), but the protein my still rotate as a consequence of the rotation of the particle. A useful approach to analyze the combined effect of the three potential depolarizing processes (local tryptophan rotation, global protein rotation and particle rotation) is the approach presented by Solleilet (28). If the three types of rotation are assumed to occur independently the total anisotropy can be written as a product of three corresponding depolarizing factors $d_i$ (26)

$$r = r_o \cdot d_{Trp} \cdot d_{prot} \cdot d_{part} = r_o \cdot [1+\tau/\theta_{Trp}]^{-1} \cdot [1+\tau/\theta_{prot}]^{-1} \cdot [1+\tau/\theta_{part}]^{-1} \qquad (9)$$

The rotational correlation time $\theta_{part}$ for the particle can be estimated by using (6) with the particle radius $R_{part} = D/2$ where $D$ is the average particle diameter (See Table 2). Even for the smallest particles studied here (MPS-40) the rotation time $\theta_{part}$ is as long as 8.5 μs (Table 2), so $d_{part}$ = 1 in equation (9) since τ is only a few ns. It means that all particles studied here can be viewed as non-rotating on the time scale of the tryptophan fluorescence lifetime. Disregarding for the moment the potential tryptophan segmental motion (i.e. setting $d_{Trp}$ = 1 in equation (9)), the anisotropy is given by $r = r_o \cdot d_{prot}$. If the protein is adsorbed rigidly to the pore wall (or to

the external particle surface) $d_{prot}$ = 1 and the predicted value of the anisotropy is then $r = r_o$ = 0.3. Below we discuss the potential contribution to the measured anisotropy from segmental motion of the tryptophan residues, in addition to the overall protein rotation.

## 3. Results and discussion

We use fluorescence anisotropy to monitor the rotation of the proteins, lipase (MML) and albumin (BSA) when they are inside the pores of the MPS particles in Table 2, with the aim to compare with their rotation rates in free solution. Since the rotational motion in the pores may be retarded if the immobilized protein concentrations are non-dilute (equation (7)) we have also measured the amount of protein taken up by the particles. Finally we discuss three possible mechanisms behind the change of anisotropy in the presence of the particles.

### 3.1. Fluorescence anisotropy

The two types of MPS-2000 particles in Table 2 were used to study the effect of pore size, whereas the four MPS-samples with approximately the same pore diameter (8.9 – 9.3 nm) were used to investigate the effect of particle size and shape (See Figure1) for a given pore size.

**Effect of pore size.** Table 3 compares the measured steady state anisotropy ($r$) of free protein with the same protein when immobilized in MPS-2000 particles of two different average pore sizes. The first observation is that both MML and BSA exhibit an anisotropy in the presence of the particles which is significantly higher compared to the same enzyme in free solution (given the uncertainty ±0.01 in the $r$ - values), which indicate a slower protein rotation inside the pores, or possibly due to adsorption on the external particle surface. (Non-immobilized protein has been removed by our washing protocol, see Methods). Secondly, the anisotropy in the presence of the particles is significantly lower than the limiting value of $r_o$ = 0.3 which would be expected if the proteins are rigidly bound to the pore walls or external particle surface (due to the slow rotation of the particles themselves, see Theory).

**Table 3. Fluorescence anisotropy of free and immobilized proteins in particles with different pore size**

| | | MML | | BSA | |
|---|---|---|---|---|---|
| **Particle type** | $R_{pore}$[b] (nm) | r[c] | $\theta_A$[d] (ns) | r[c] | $\theta_A$[d] (ns) |
| Free protein[a] | ---- | 0.06 | 0.87 | 0.09 | 2.73 |
| MPS-2000 | 4.5 | 0.17 | 4.58 | 0.18 | 9.45 |
| MPS-2000 | 3.0 | 0.21 | 8.17 | 0.24 | 25.20 |

a. Protein in particle-free buffer solution.
b. Pore radius
c. Measured steady state anisotropy. The uncertainty is ±0.01 as calculated from the variation between 3 to 4 independent experiments.
d. Apparent rotational correlation time calculated from steady state anisotropy (*r*) by equation (5).The uncertainty is ±0.2ns from the variation between 3 to 4 independent experiments.

The observed *r*-values are intermediate between free and fully adsorbed proteins, which strongly indicates that the proteins do undergo some depolarizing motion inside the pores, but which is retarded compared to the free protein. This interpretation is supported by the observation that for a given protein the anisotropy is higher in the more narrow pores, as expected since stronger confinement is likely to affect the motion more strongly. We also note that non-immobilized MML has a lower anisotropy value than free BSA, consistent with that the smaller MML ($R_H$ = 2.25 nm) rotates faster in free solution than BSA ($R_H$ = 3.5 nm) in agreement with well-established results. Taken together these observations indicate that tryptophan fluorescence anisotropy can be used for studying the rotation of immobilized enzymes in a manner similar to free proteins.

**Effect of particle type and size.** Table 4 shows the anisotropy for MML and BSA when they are immobilized in MPS particles with different size but approximately the same pore size, $R_{pore}$ = (4.6±0.2) nm. Again it is seen that with all four types of MPS particles studied here the immobilized MML and BSA have significantly higher anisotropy values compared to the same free enzymes, consistent with that immobilization reduces the rotational motion of both MML and BSA.

**Table 4. Fluorescence anisotropy of proteins immobilized in different particles types with the same pore size**

| | MML | | BSA | |
|---|---|---|---|---|
| **Particle type** [a] | $r^c$ | $\theta_A{}^d$ (ns ) | $r^c$ | $\theta_A{}^d$ (ns ) |
| Free protein[b] | 0.06 | 0.87 | 0.09 | 2.73 |
| MPS-40 | 0.23 | 11.5 | 0.18 | 9.45 |
| MPS-300 | 0.30 | ----- | 0.27 | 56.70 |
| MPS-1000 | 0.15 | 3.50 | 0.16 | 7.24 |
| MPS-2000 | 0.17 | 4.58 | 0.18 | 9.45 |

a. MPS-*D* where *D* is the average particle diameter in nm. The pore radius is approximately the same at 4.6+/-0.2 nm (for exact values see Table 2)
b. Protein in particle-free buffer solution
c. Measured tryptophan steady state anisotropy. The uncertainty is ±0.01 as calculated from the variation between 3 to 4 independent experiments.
d. Apparent rotational correlation time calculated from anisotropy by equation (5). The uncertainty is ±0.2ns from the variation between 3 to 4 independent experiments.

In Table 4, there is no trend in the anisotropy values with particle size, in accordance with that even the smallest particles are too large to undergo any depolarizing rotation during the tryptophan fluorescence lifetime ($\theta_{part} >> \tau$). The difference in anisotropy between different particle types is, therefore, most likely due to their different morphology, or possibly to differences in protein-particle interaction strength. Interestingly, in MPS-300, MML exhibits the limiting anisotropy value $r_o$ = 0.3, indicating essentially non-moving proteins, and BSA gives almost the same value ($r$ =0.27) in the same type of particle. For the other particle types in Table 4, the measured anisotropy is in an intermediate range (0.15-0.23) which again indicates that the proteins are able to rotate inside the pores, albeit more slowly than in free solution. Figure S1 summarizes the combined data of Tables 3 and 4 in terms of the measured anisotropy *vs* ratio between protein and pore average radii, and the overall results suggest that the anisotropy tends to increase with relative pore narrowness, and that MPS-300 seemingly deviates from this trend.

## 3.2. Protein loading and pore filling

The amount of immobilized proteins in porous particles is commonly expressed as the mass of protein bound per gram of (dry) particles, or protein loading ($P_{LD}$). Table 5 shows the degree of immobilization *DOI* (the fraction of the added proteins which remain bound to the particles), and the resulting protein loadings obtained for all the combinations of proteins and particles in this study.

**Table 5. Protein loading in the MPS particles**

| | | MML | | | BSA | | |
|---|---|---|---|---|---|---|---|
| **Particle type**[a] | $R_{pore}$[b] *(nm)* | *DOI*[c] *(%)* | $P_{LD}$[d] (µg/mg) | $P_f$[e] | *DOI*[c] *(%)* | $P_{LD}$[d] (µg/mg) | $P_f$[e] |
| MPS-40 | 4.5 | 72 | 288 | 0.284 | 84 | 336 | 0.604 |
| MPS-300 | 4.7 | 75 | 300 | 0.261 | 87 | 348 | 0.553 |
| MPS-1000 | 4.6 | 70 | 280 | 0.213 | 85 | 340 | 0.472 |
| MPS-2000 | 4.5 | 71 | 284 | 0.218 | 84 | 336 | 0.470 |
| MPS-2000 | 3.0 | 63 | 252 | 0.209 | 38 | 152 | 0.230 |

a. MPS-*D*, where *D* indicates average particle diameter in nm (see Table 2).
b. Average pore radius
c. Degree of immobilization, fraction of added proteins which were immobilized.
d. Protein loading (µg protein per mg of dry particles)
e. Pore filling from equation (1).

It is seen from Table 5 that the *DOI*-values are essentially constant (72±2% for MML and 85±2% for BSA) for the four different particle types with a pore radius of 4.5-4.7 nm. That the particle size has little influence on protein loading has been reported before (21), although the amount of loaded protein obtained here is higher probably because the added amount of protein per particle was four times higher than in the previous study (7, 21). We have not determined the full binding isotherms for the immobilization, but the DOI-numbers in Table 5 suggest that this set of particles are saturated with protein under our conditions. The high loading of both

proteins shows that the pore size of around 4.5 nm is suitable for immobilization of proteins in the present size range, probably because the hydrodynamic radius of MML and BSA are smaller than but comparable to the pore size. It has also been reported that the pore size is important for enzymatic activity, and $R_{pore}$ = 4.4nm was found to give both high loading and high enzymatic activity for MML (7).

When comparing the two types of MPS-2000 particles, the degree of immobilization and protein loading is considerably lower for the particles with the smaller pore size, especially for the larger BSA. In the case of MML this observation is in agreement with a previous study with the same type of particles (7) and consistent with that less space is available inside the MPS with the smaller pore diameter. Nominally BSA ($R_H$ = 3.5 nm) is too large to enter these smaller pores ($R_{pore}$ = 3.0 nm) so a low protein loading is expected. However, complete exclusion from the pores and only binding to the external surface seems unlikely for two reasons. Firstly, if the proteins are only immobilized by binding to the external surface their anisotropy is expected to be 0.3 (as is observed with MPS-300 in Table 4), and the significantly lower value of 0.24±0.01 (Table 3) indicates the presence of some protein mobility which is seemingly inconsistent with permanent adsorption (although internal protein dynamics may still cause some depolarization). Secondly, the amount of immobilized protein (152 µg/mg) would correspond to roughly 8 layers of close-packed proteins bound on the external surface of the 2000nm particles (results not shown). The driving force for such a protein-protein driven immobilization is unclear, and should occur also with the other particle types. In fact, with an experimental width in the pore size distribution of typically 10% of the mean pore size (7) the particles can be expected to contain a fraction of pores large enough to house the BSA, especially considering that the effective size of BSA in terms of its density is $R_{eff}$ = 2.7nm (29). For the larger pore size (mean value 4.5 nm) almost the whole pore distribution is accessible also to BSA, consistent with the

two-fold higher loading (336 µg/mg) which is the same as for the smaller particles with the same pore size.

The rotational diffusion of a protein solution is expected to be retarded by high protein concentrations, as described by equation (7) in terms of the protein volume fraction $\phi$. It is then illustrative to use equation (1a) to convert the protein loading values into pore filling ($P_f$), which shows how large fraction of the pore volume that is occupied by the immobilized proteins. The $P_f$-values presented in Table 5 shows that generally MML fills a significantly smaller fraction of the available pore volume (volume fraction $\phi$ = 20-30%) than BSA ($\phi$ = 50-60%).

The results on the degree of pore filling is best understood in terms of the average number of proteins per particle $N_{prot}$ (see Table 6) calculated by applying equation (1b) to the data in Table 5. It is seen that for the MPS-40 there is only about 100 protein per particle on the average, and that $N_{prot}$ increases with increasing particle size as expected.

**Table 6. Average number of proteins per particle**

| | | $N_{prot}$[a] | | |
|---|---|---|---|---|
| **Particle type**[b] | $R_{pore}$[c] *(nm)* | MML | BSA | MML/BSA[d] |
| MPS-40 | 4.5 | 133 | 75 | 1.77 |
| MPS-300 | 4.7 | $5.4 \cdot 10^4$ | $3.0 \cdot 10^4$ | 1.78 |
| MPS-1000 | 4.6 | $1.7 \cdot 10^6$ | $9.9 \cdot 10^5$ | 1.70 |
| MPS-2000 | 4.5 | $1.4 \cdot 10^7$ | $7.9 \cdot 10^6$ | 1.74 |
| MPS-2000 | 3.0 | $1.3 \cdot 10^7$ | $3.8 \cdot 10^6$ | 3.42 |

a. Average number of proteins per particle from equation (1b) and data in Table 5
b. MPS-*D*, where *D* indicates average particle diameter in nm
c. Pore radius
d. Ratio of number of MML and BSA proteins per particle.

From Table 6 it is seen that the number of MML per particle is a factor of 1.75+/-0.03 higher than for BSA for all the four particle types with the large (4.6 nm) pores, explaining the higher pore filling with BSA since the volume of each BSA is 3.8 times larger compared to the MML molecule and therefore is more efficient at filling the pores. In a deviation from this overall pattern BSA has a pore filling of only 23% in the MPS-2000 particles with the small pores and

thereby nearly as low as for MML, which is due to that the number of MML is now about 3.4 higher than BSA, almost exactly compensating for its smaller volume per protein. The highest volume fractions measured here (0.6) is below but approaching the theoretical upper limit for close packing of spheres in a cylindrical pore (0.67), but more detailed comparison with theories for packing of proteins (spheres) in particle pores (reviewed in Carlsson et al (22)) need more extensive characterization of the immobilization binding isotherms.

Figure 4 shows a plot of the values of $N_{prot}$ for all particles in Table 6 versus particle size, and the strong increase shows that the larger particles accommodate many more proteins. In fact, the inset in Figure 4 shows that the number of protein per particle (with the same pore size) scales with the linear particle size $D$ as $N_{prot} \sim D^{2.94+/-0.01}$ for MML and $N_{prot} \sim D^{2.95+/-0.01}$ for BSA. The nearly cubic scaling (i.e scaling with particle volume) supports the proposal that under our immobilization conditions both proteins essentially saturate the particle, and secondly that they are evenly distributed which justifies that the average experimental $P_f$ -values (Table 5) can be used for the volume fraction ($\phi$) in equation (7).

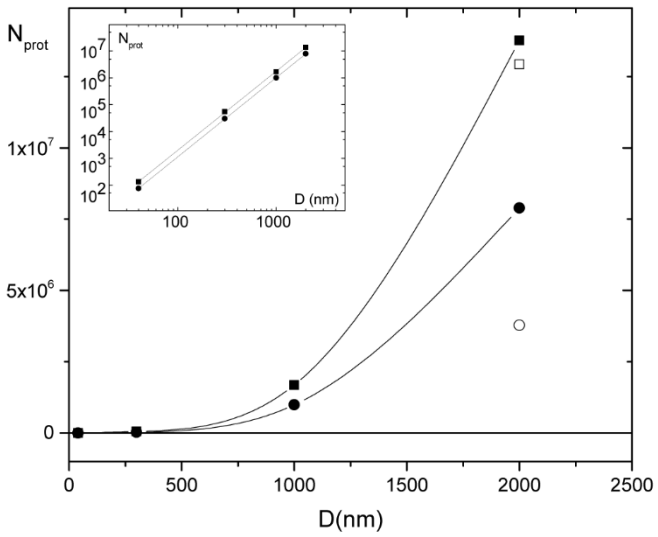


Figure 4. The average number of proteins per particle for MML (squares) and BSA (circles) versus the average particle diameter $D$, for pore radius 4.6+/-0.2 nm (solid symbols; curves are guide to eye) and 3.0nm (open). Inset: Double logarithmic plot for data with 4.6 nm pore radius where straight lines are least square linear fits giving slopes 2.94+/-0.02 for MML and 2.95+/-0.01 for BSA.

## Mechanisms of enhanced protein anisotropy in the pores.

The enhanced protein anisotropy in the presence of the particles (Tables 3 and 4; Figure S1) reveals a retardation of either the rotational motion of the whole protein or the local motion of the tryptophan residues (depolarization factors $d_{prot}$ and $d_{Trp}$ in equation (9) respectively), or both. In the steady state anisotropy technique employed here these two contributions are convoluted into an apparent rotational correlation time ($\theta_A$) which is significantly larger in the pores than for free protein (Table 3 and 4), an observation which just reflects the anisotropy results in terms of a time scale. Here we will discuss three possible mechanisms of retardation in the pores, and while noticing that all of them may affect also the internal tryptophan motion we focus on the global rotation in an attempt of a semi-quantitative evaluation of the relative importance of the three mechanisms. A fully quantitative comparison with the underlying theories will require time-resolved anisotropy measurements, which can be used to resolve the two types of motion (11) because the local tryptophan motion occurs on considerably shorter time scales (a few ns) than for overall rotation of proteins which is estimated to occur over tens of ns for the two proteins studied here (see $\theta_{prot\ free}$ in Table 1).

One obvious retardation mechanism is that protein rotation is fully hindered due to permanent attachment to the pore wall, but then an anisotropy of 0.3 is expected because the particles used here are in effect stationary on the time scale of tryptophan fluorescence lifetime. The anisotropies we measure are significantly lower, except for MML in MPS-300 (Table 4). For this particle type wall-adsorption cannot be ruled out, and interestingly Gustafsson et al have noted a different activity of lipase in these type of particles (21) perhaps due to a different type of interaction with the pore walls. Both proteins are negatively charged at the pH 6 used here, so the electrostatic interaction with the negatively charged silica pore wall plays approximately the same role for a given protein. For the other particle types it seems another retarding

mechanism needs to be invoked, although presently we cannot fully exclude permanently adsorbed protein which retain some local tryptophan depolarizing motion.

A second possibility is retardation of protein rotation by protein-protein (hydrodynamic) interactions at the high degree of pore filling we observe (Table 5), and according to equation (7) the maximum expected retardation by this mechanism is for BSA in MPS-40 ($\phi = 0.604$ in Table 5) and then by a factor of 1.6. The measured retardation factor for $\theta_A$ compared to free BSA is about twice as high at a factor of 3.5 (Table 4). Furthermore, the slight but monotonously decreasing pore filling seen with both MML and BSA with increasing particle size (at constant pore size; Table 5) is not reflected in a similar trend of monotonously decreasing anisotropy values (Table 4). Finally, for both MML and BSA the anisotropy is higher in the more narrow pores (Table 3) even though the pore filling is lower (Table 5). It therefore seems unlikely that a protein-protein induced retardation of the overall rotation in the pores by itself can explain the enhanced anisotropies we observe in the presence of the particles. Notably equation (7) does not include potential effects of hydrodynamic protein-protein interactions on the internal protein dynamics in non-dilute solutions. Such effects have not been studied under present ambient conditions to our knowledge, but it is interesting that enhanced protein-protein interactions at elevated pressures tend to partly quench internal motion in lysozyme (30). An indirect effect of high protein concentration is the possibility of formation of dimers (or higher protein aggregates) which result in enhanced anisotropy due to an increased radius in equation (6). However, a quasi-elastic neutron scattering study of BSA translational diffusion in non-dilute solutions (29) showed no indication of dimer formation at least up to protein volume fractions of 0.35, since the results were well described by monomer diffusion retarded by protein-protein hydrodynamic interactions. The results were corrected for a contribution to the neutron scattering from rotational diffusion, but unfortunately no results on the effect of protein crowding on BSA rotation was presented.

A third possible retarding mechanism is hydrodynamic interactions with the pore walls, which according to the theoretical work by Jones for a spherical particle confined between two planar walls (31) typically affect particle diffusion up to a few particle radii from the pore wall and hence can be expected to play a role in our system since protein and pore radii are comparable. Importantly such a mechanism will operate even if the protein solution in the pores is dilute, and thus may not necessarily be in conflict with our observed (lack of) trends in anisotropy with the degree of pore filling. Jones (31) finds that rotational diffusion is considerably less retarded than translation however, so even very close to the wall in a channel twice as wide as the particle diameter (corresponding to $D/2R_H = 2$ in our system) the rotational diffusion coefficient $D_{rot}$ is lower than in free solution only by a factor of about 0.5-0.8 (depending on the orientation of the rotation axis relative to the surface). This prediction is in qualitative agreement with a resonance enhanced dynamic light scattering study of gold rods near a solid surface (32), where $D_{rot}$ is reported to be lower by a factor of about 0.5 compared to the same particle far from the surface. Converted into the average rotational correlation time we measure by fluorescence anisotropy the prediction by Jones corresponds to an increased $\theta_{rot}$ by a factor of about 1.7, and hence less than the increase in $\theta_A$ by a factor of 0.17/0.06 = 2.8 we observe in the case of MML in the wider pores (Table 3) for which situation the relative pore width $D/2R_H = 2$ is the same as the relative slit width used by Jones. Notably, our proteins will most likely be radially distributed in the pore at the moment of excitation so the ensemble averaged retardation of the rotation will be weaker than predicted closest to the wall, but this effect will be partially offset by the fact that in a cylindrical pore they are surrounded by walls on all sides in contrast to the slit model used by Jones. Hence, also the wall-particle interaction model underestimates the retardation slightly, but again we note that the model by Jones (31) does not include the effect of hydrodynamic interactions with a solid surface on the internal dynamics of a protein. Such effects have to our knowledge not been studied for proteins immobilized in rigid pores, but

Simorellis and Flynn (33) have used NMR relaxation measurements to study the internal dynamics of ubiquitin encapsulated in AOT/water reversed micelles with a water pool diameter of about 8.5 nm (34), and thus comparable to our largest pore diameters. They report that such nanometer scale confinement of the protein retards the motion of particularly flexible residues also on the ns time scale probed by fluorescence, albeit unfortunately without information regarding the particular case of tryptophan residues which is lacking in human ubiquitin.

## 4. Conclusion

At the present level of experimental accuracy the comparison with possible retardation mechanisms indicates that the magnitude of the retardation is slightly larger than predicted by hydrodynamic interactions between protein and pore wall, as well as between the proteins themselves at the non-dilute concentrations we measure in the pores. One possibility is that both mechanisms contribute, in fact a coupling of the two types of hydrodynamic interactions would not be surprising in the narrow pores, but verification will require further studies by time-resolved anisotropy (to ascertain the effect of immobilization on internal protein motion) performed in a range of volume fractions (to ascertain the role played by protein-protein interactions). The combined immobilization effects on global and internal protein dynamics are complicated, but understanding them separately may help to explain how immobilization in MPS may affect enzymatic activity in as much as the activity depends on how free the protein is to undergo local dynamics.

## 5. Acknowledgements.

Hanna Gustafsson is thanked for synthesis and characterization of all the MPS particles. A Linnaeus grant SUPRA to B.Å from the Swedish Research Council is thankfully acknowledged.

# References:


1. Lee C-H, Lin T-S, Mou C-Y. Mesoporous materials for encapsulating enzymes. Nano Today. 2009;4(2):165-79.
2. Lei CH, Shin YS, Liu J, Ackerman EJ. Entrapping enzyme in a functionalized nanoporous support. Journal of the American Chemical Society. 2002;124(38):11242-3.
3. Hudson S, Cooney J, Magner E. Proteins in Mesoporous Silicates. Angew Chem-Int Edit. 2008;47(45):8582-94.
4. Lei CH, Soares TA, Shin YS, Liu J, Ackerman EJ. Enzyme specific activity in functionalized nanoporous supports. Nanotechnology. 2008;19(12):9.
5. Nabavi Zadeh PS, Mallak KA, Carlsson N, Åkerman B. A fluorescence spectroscopy assay for real-time monitoring of enzyme immobilization into mesoporous silica particles. Analytical biochemistry. 2015;476:51-8.
6. Thorn C, Gustafsson H, Olsson L. QCM-D as a method for monitoring enzyme immobilization in mesoporous silica particles. Microporous and Mesoporous Materials. 2013;176:71-7.
7. Gustafsson H, Thörn C, Holmberg K. A comparison of lipase and trypsin encapsulated in mesoporous materials with varying pore sizes and pH conditions. Colloids and Surfaces B: Biointerfaces. 2011;87(2):464-71.
8. Thörn C, Carlsson N, Gustafsson H, Holmberg K, Åkerman B, Olsson L. A method to measure pH inside mesoporous particles using protein-bound SNARF1 fluorescent probe. Microporous and Mesoporous Materials. 2013;165:240-6.
9. Yamaguchi A, Namekawa M, Kamijo T, Itoh T, Teramae N. Acid−Base Equilibria inside Amine-Functionalized Mesoporous Silica. Analytical chemistry. 2011;83(8):2939-46.
10. Careri G, Fasella P, Gratton E. Enzyme Dynamics: The Statistical Physics Approach. Annual Review of Biophysics and Bioengineering. 1979;8(1):69-97.
11. Lakowicz JR, Maliwal B, Cherek H, Balter A. Rotational freedom of tryptophan residues in proteins and peptides. Biochemistry. 1983;22(8):1741-52.
12. Jameson DM, Ross JA. Fluorescence Polarization/Anisotropy in Diagnostics and Imaging. Chemical Reviews. 2010;110(5):2685-708.
13. Lakowicz JR. Fluorescence spectroscopic investigations of the dynamic properties of proteins, membranes and nucleic acids. Journal of Biochemical and Biophysical Methods. 1980;2(1–2):91-119.
14. Ingersoll CM, Strollo CM. Steady-State Fluorescence Anisotropy To Investigate Flavonoids Binding to Proteins. Journal of Chemical Education. 2007;84(8):1313.
15. González Flecha FL, Levi V. Determination of the molecular size of BSA by fluorescence anisotropy. Biochemistry and Molecular Biology Education. 2003;31(5):319-22.
16. Lakowicz JR. Principles of Fluorescence Spectroscopy. 3rd ed. Baltimor, USA: Springer; 2006.
17. Wu XY, Jaaskelainen S, Linko YY. Purification and partial characterization of Rhizomucor miehei lipase for ester synthesis. Appl Biochem Biotechnol. 1996;59(2):145-58.
18. Hirayama K, Akashi S, Furuya M, Fukuhara K. Rapid confirmation and revision of the primary structure of bovine serum albumin by ESIMS and Frit-FAB LC/MS. Biochemical and biophysical research communications. 1990;173(2):639-46.
19. Graupner M, Haalck L, Spener F, Lindner H, Glatter O, Paltauf F, et al. Molecular Dynamics of Microbial Lipases as Determined from Their Intrinsic Tryptophan Fluorescence. Biophysical Journal. 1999;77(1):493-504.
20. Joshi NV, Joshi VOd, Contreras S, Gil H, Medina H, Siemiarczuk A, editors. Fluorescence lifetime measurements of native and glycated human serum albumin and bovine serum albumin1999.
21. Gustafsson H, Johansson EM, Barrabino A, Odén M, Holmberg K. Immobilization of lipase from Mucor miehei and Rhizopus oryzae into mesoporous silica—The effect of varied particle size and morphology. Colloids and Surfaces B: Biointerfaces. 2012;100(0):22-30.
22. Carlsson N, Gustafsson H, Thörn C, Olsson L, Holmberg K, Åkerman B. Enzymes immobilized in mesoporous silica: A physical–chemical perspective. Advances in Colloid and Interface Science. (0).

23. Haynes WM, Lide DR. CRC handbook of chemistry and physics : a ready-reference book of chemical and physical data. Boca Raton, Fla.: CRC Press; 2011.
24. Ando T, Skolnick J. Crowding and hydrodynamic interactions likely dominate in vivo macromolecular motion. Proceedings of the National Academy of Sciences. 2010;107(43):18457-62.
25. Banchio AJ, Nägele G. Short-time transport properties in dense suspensions: From neutral to charge-stabilized colloidal spheres. The Journal of Chemical Physics. 2008;128(10):104903.
26. Lakowicz JR, Freshwater G, Weber G. Nanosecond segmental mobilities of tryptophan residues in proteins observed by lifetime-resolved fluorescence anisotropies. Biophys J. 1980;32(1):591-601.
27. B. Massey J, Churchich JE. Nanosecond spectroscopy of a dimeric enzyme: plasma amine oxidase. Biophysical Chemistry. 1979;9(2):157-62.
28. Soleillet P. Sur les parametres caractérisant la polarisation partielle de la lumiere dans les phénomenes de fluorescence: Ann.Phys.Biol.Med; 1929.
29. Roosen-Runge F, Hennig M, Zhang F, Jacobs RMJ, Sztucki M, Schober H, et al. Protein self-diffusion in crowded solutions. Proceedings of the National Academy of Sciences. 2011;108(29):11815-20.
30. Erlkamp M, Marion J, Martinez N, Czeslik C, Peters J, Winter R. Influence of Pressure and Crowding on the Sub-Nanosecond Dynamics of Globular Proteins. The Journal of Physical Chemistry B. 2015;119(14):4842-8.
31. Jones RB. Rotational diffusion of colloidal particles near confining walls. The Journal of Chemical Physics. 2005;123(16):164705.
32. Haghighi M, Tahir MN, Tremel W, Butt H-J, Steffen W. Translational and rotational diffusion of gold nanorods near a wall. The Journal of Chemical Physics. 2013;139(6):064710.
33. Simorellis AK, Flynn PF. Fast Local Backbone Dynamics of Encapsulated Ubiquitin. Journal of the American Chemical Society. 2006;128(30):9580-1.
34. Kinugasa T, Kondo A, Nishimura S, Miyauchi Y, Nishii Y, Watanabe K, et al. Estimation for size of reverse micelles formed by AOT and SDEHP based on viscosity measurement. Colloids and Surfaces A: Physicochemical and Engineering Aspects. 2002;204(1–3):193-9.